Constructing Metastructures with Broadband Electromagnetic Functionality

Ren-Hao Fan, Bo Xiong, Ru-Wen Peng,* and Mu Wang*

Electromagnetic metastructures stand for the artificial structures with a characteristic size smaller than the wavelength, which may efficiently manipulate the states of light. However, their applications are often restricted by the bandwidth of the electromagnetic response of the metastructures. It is therefore essential to reassert the principles in constructing broadband electromagnetic metastructures. Herein, after summarizing the conventional approaches for achieving broadband electromagnetic functionality, some recent developments in realizing broadband electromagnetic response by dispersion compensation, nonresonant effects, and several trade-off approaches are reviewed, followed by some perspectives for the future development of broadband metamaterials. It is anticipated that broadband metastructures will have even more substantial applications in optoelectronics, energy harvesting, and information technology.

1. Introduction

Controlling the states of light is an important issue in nanophotonics. Metastructures[1–8] possess artificially designed subwavelength units, and can effectively affect the propagation of light. Metamaterials[2–6] and metasurfaces[7,8] are well-known examples in three-dimensional (3D) and two-dimensional (2D) scenarios, respectively. By carefully designing geometrical structures and chemical constituents,[6] metastructures can possess unique optoelectric features that are unavailable in conventional materials, such as near-zero or negative refractive index. Due to the unique capability to tune the propagation direction, amplitude, and polarization state of the light, in principle, the metastructures can replace traditional bulky and heavy optical devices, and hence benefit the integration and miniaturization of optical devices. However, practically, due to the intrinsic dispersion of materials (e.g., normal chromatic dispersion of dielectrics[9] and intrinsic dispersion of metals[10,11]) and the resonant feature of some metastructures,[4,6] many fascinating physical properties

occur only at specific frequencies. Such a narrow-bandwidth feature dramatically restricts the application of the metastructures to versatile areas, such as display technology, optoelectronics, communications, energy harvesting, etc. For example, since the solar spectrum extends from about 0.29 to over 3.2 µm, for the efficient application of solar energy conversion, a broadband responsive system is an essential step in realizing the high-efficiency solar energy harvesting.[12] Bandwidth is an important issue in display technology as well. Full-color hologram and imaging in virtual reality and augmented reality systems require the modulation over the whole spectrum. However, most of the existing holograms nowadays can only exhibit monochromatic holograms or the images with limited primary colors due to the strong angular dispersion of the diffractive optical elements.[13] Currently, chromatic aberration remains a serious challenge for full-color holograms.

So far, great efforts have been devoted to broadening the frequency range of the electromagnetic response of metastructures. The most straightforward approach is to superimpose different resonant modes in the system. For example, the bandwidth of a metamaterial absorber[14] can be expanded by combining several individual resonant modes with different frequencies. Essentially, this superposition approach requires simultaneous excitations at all the resonant frequencies in the metastructures, and this requirement confines the final bandwidth of this approach.

The unique advantage of the artificially structured materials is that their band structure and dispersion relation can be accurately tuned. It has been demonstrated that upon illumination of the incident light, the surface charge density waves can be excited on the metallic surface, which are usually known as surface plasmons (SPs). The surrounding electromagnetic field is hence modulated by the irradiation of the oscillating surface plasmon. At the resonant frequency, this effect becomes so strong that a thin metallic metastructure can effectively tune the state of light.[7,8] However, the underlying Drude–Lorentz response of the permittivity of metal is highly dispersive, which limits its application to the specific resonant frequency of the surface plasmon.[1] On the other hand, dielectric material interacts with light in a much gentle way that the influence to light is represented by the accumulation of optical path over a certain thickness.[11] This

Dr. R.-H. Fan, B. Xiong, Prof. R.-W. Peng, Prof. M. Wang
National Laboratory of Solid State Microstructures, School of Physics, and Collaborative Innovation Center of Advanced Microstructures
Nanjing University
Nanjing 210093, China
E-mail: rwpeng@nju.edu.cn; muwang@nju.edu.cn

The ORCID identification number(s) for the author(s) of this article can be found under https://doi.org/10.1002/adma.201904646.

**ADVANCED
SCIENCE NEWS**
www.advancedsciencenews.com

**ADVANCED
MATERIALS**
www.advmat.de

feature is effective over a broad bandwidth and has already been applied in antireflection coating and many other optical devices.[10,15] By combining a metallic metastructure and a dielectric interlayer, it is possible to realize a dispersion-free broadband device, where the strong response of the metallic structures helps to decrease the device size and the dielectric interlayer compensates the dispersion simultaneously in both the amplitude and the phase difference of light.[16–18] The physical picture of this process is straightforward: by superimposing the metallic metastructures and dielectric interlayer, the intrinsic dispersion generated by the resonance of metallic structures is compensated by the interlayer thickness-sensitive dispersion of the dielectric interlayer, so the dispersion-free optical functionalities can be realized in a limited space.

Another way to achieve the dispersion-free feature is to select a working frequency far away from the resonant frequency, where the dispersion spectrum is nearly flat, and the permittivity and permeability do not change significantly with the frequency of the incident light. This scenario is similar to that of the dielectric material, where the interaction with the electromagnetic waves is weak. Consequently, the material should be sufficiently thick to affect the states of electromagnetic waves. This type of metamaterial is usually designated as a nonresonant metamaterial.[19]

In addition to the aforementioned approaches, there are several trade-off approaches in realizing the broadband response. At the resonance of the metastructures, the dimensionless Q factor, which stands for the ratio of the resonant frequency to the full width at half maximum (FWHM), characterizes the relationship between the bandwidth with respect to its center frequency. By lowering the Q factor at the resonant frequency, the energy will dissipate more quickly and consequently the bandwidth broadens. Another example comes from ultrafast optics. According to the Fourier transformation, a narrow wave packet in the time domain corresponds to a broad coverage in the frequency domain. This means that a broadband frequency response can be realized by applying ultrafast optical pulses.

Herein, we first provide a brief review of the principles in designing metamaterials with broadband electromagnetic functionality, followed by analyzing the characteristics of each method. Finally, perspectives are given on the development of broadband metamaterial design. The structure of the paper is illustrated in **Figure 1**. After a brief review of the different approaches to realize the broadband electromagnetic responses, we describe respectively the design principles, advantages, and limitations of these different approaches in detail. In Section 2.1, the broadband response realized by combining multiple resonant modes is discussed; in Section 2.2, the dispersion compensation approach based on metal–dielectric materials is reviewed; Section 2.3 focuses on the nonresonant effect of the metastructures; and in Section 2.4, the broadband response realized by using some trade-off approaches, such as lowering the Q factor and introducing ultrafast systems, are presented. In Section 3, we try to summarize the trend in developing new metamaterial to meet the different demands for the broadband responses.

Ren-Hao Fan is an associate professor at Nanjing University. He received his Ph.D. from Nanjing University in 2013 and worked as a postdoctoral researcher at Nanjing University. In 2016, he joined the School of Physics, Nanjing University. His research interests include metamaterials, terahertz technology, nanophotonics, and plasmonics.

Ru-Wen Peng received her Ph.D. in condensed matter physics from Nanjing University in 1998. Currently, she is a distinguished professor at Nanjing University and a principal investigator at National Laboratory of Solid State Microstructures at Nanjing University. Her current research interests include plasmonics and nanophotonics, metamaterials, photonic quasicrystals, phononic transport, and heat transfer in nanostructures.

Mu Wang received his Ph.D. in condensed matter physics from Nanjing University in 1991. He is the Cheung-Kong Professor of Physics in School of Physics and the National Laboratory of Solid State Microstructures of Nanjing University. His research interests include nanophotonics, metamaterials, physics of interfacial growth and fabrication technology.

2. The Scheme of Broadband Electromagnetic Response Implementation

2.1. Broadband Response Based on Combining Multiple Resonant Modes

In this section, we focus on the conventional approach to realize the broadband electromagnetic functionality with the
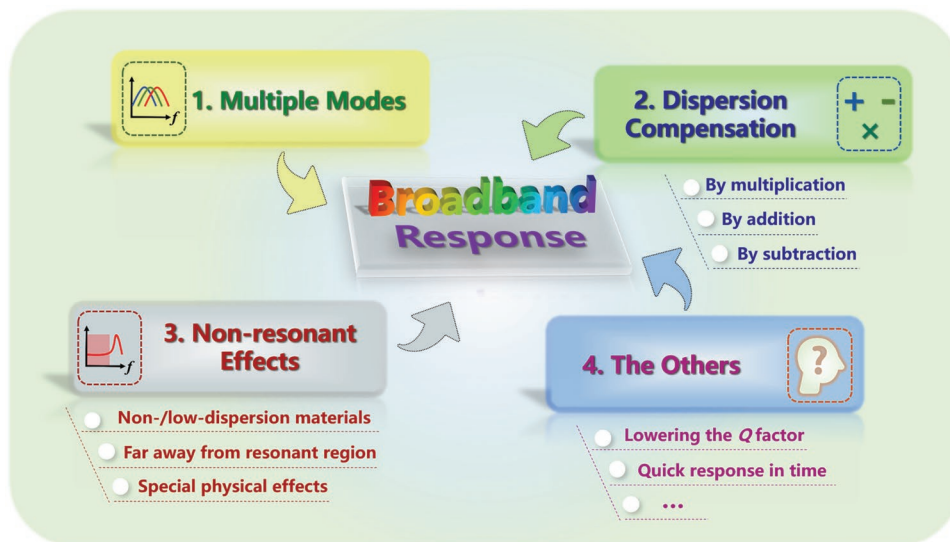
Figure 1. The schematics to show different approaches in realizing broadband electromagnetic functionality with metastructures, including superimposing multiple resonant modes, dispersion compensation via the multiplication, addition, or subtraction of the contributions from different dispersion, several nonresonant effects, and some trade-off approaches, such as lowering the Q factor and introducing ultrafast systems.

artificially structured materials, which is based on superimposing multiple resonant modes in the system, as illustrated in **Figure 2**. It is noteworthy that the bandwidth of each resonance is narrow. Superimposing multiple resonant modes with different resonant frequencies can realize the broadband feature. The examples can be found in various branches of photonics, such as absorbers,[14] antennas,[20,21] filters,[22,23] scatterers,[24] reflectors,[25] invisibility cloaks,[26,27] negative-refractive-index metamaterials,[28,29] slow-light metamaterials,[30–33] anomalous propagations of light,[34,35] high-refractive-index metamaterials,[36] and so on.

Here, we take the broadband absorber as an example to elucidate that superimposing multiple resonant modes can indeed achieve a broadband electromagnetic response. Two resonant modes are selected to construct a broadband absorber.[37–47] As illustrated in **Figure 3**a, the electric-field-driven inductance–capacitance (*LC*) resonator with cell "1" and cell "2" has been designed to build a broadband ultrathin absorber at microwave regime.[40] Two distinct absorption peaks occur at 5.04 GHz (cell "2") and 5.28 GHz (cell "1") with high absorbance. The superposition of these two resonant peaks provides an FWHM bandwidth of 0.42 GHz, which symbolizes a broadband microwave absorber. Another example is that Cheng et al. demonstrated a broadband terahertz absorber made of a planar array of cross-shaped structures, which is constructed by surface etching of doped silicon.[46] In this scenario, the absorption originates

from two resonant modes supported by the plasmonic cavities of the etched cross structure (Figure 3b). To expand the working bandwidth further, people may superimpose three modes,[48–57] four modes,[58–67] or even more modes[68–87] with different resonant frequencies. As illustrated in Figure 3c, a superpixel single-layer absorber contains four subunits with different sizes.[59] It turns out that for light with both transverse-electric (TE) and transverse-magnetic (TM) polarization, the FWHM for TE incident light is 37% of the center frequency, and it becomes 41% of the center frequency for TM incident light. This polarization dependence feature is mainly induced by the anisotropic arrangement of these four subunits. Further, to generate an ideal polarization-independent broadband absorber, an alternating stack of metal crosses and dielectric layers was proposed.[59] Three close-positioned resonant peaks are superimposed to form a broadband absorption plateau (Figure 3d). Such a multilayer absorber is polarization insensitive since all these single subunits are optically isotropic.

It seems that the bandwidth of the absorber can be expanded arbitrarily by adding separated subunits with different sizes. Practically, however, there are some restrictions on the scale of planar or stereo devices. For example, by incorporating more and more resonant modes in the unit cell, the size of the unit cell will increase accordingly. Yet metamaterials require that the size of the unit cell be smaller than the wavelength since only in this case each structure cannot be identified by the
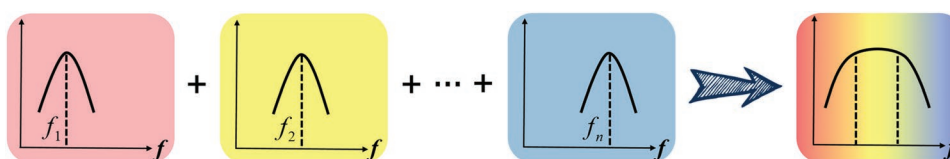

Figure 2. The schematics for achieving a broadband response by superimposing multiple resonant modes with different frequencies.
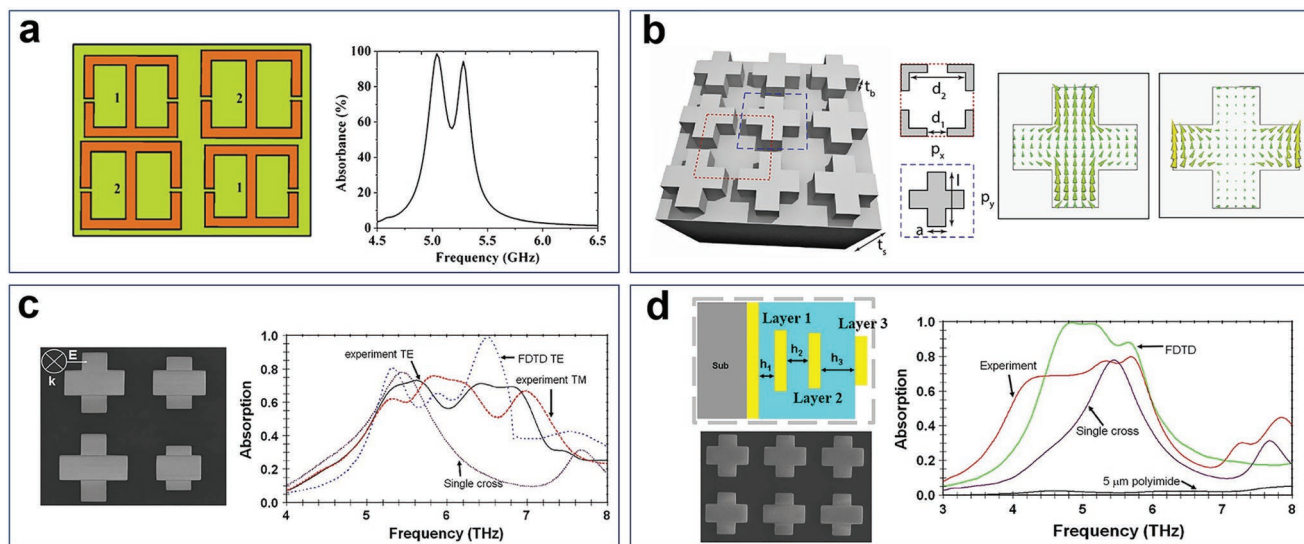
Figure 3. Superimposing different resonant modes to achieve a broadband response. a) The electric-field-driven *LC* resonator structure with cell "1" and cell "2", and the absorbance plot for normal incidence on this structure. Reproduced with permission.[40] Copyright 2013, Wiley-VCH. b) Schematic of a planar array of cross-shaped structures defined by surface etching of doped silicon, and the induced electric current density distributions on the cross structure at 0.80 THz (left column) and 1.44 THz (right column), respectively. Reproduced with permission.[46] Copyright 2015, Wiley-VCH. c) Scanning electron microscopy (SEM) image of a single superpixel of the broadband absorber, which contains four subunits with different sizes (left), and the absorption spectra for both TM and TE polarizations (right). d) Schematics to show the cross-section of a three-layered metamaterial absorber and the SEM image of the multilayer absorber with a top view (left panel). The right panel shows the experimental and simulated the finite-difference time-domain (FDTD) absorption spectra of the absorber. c,d) Reproduced with permission.[59] Copyright 2011, Optical Society of America.

electromagnetic wave and hence the material can be treated as a homogeneous one with effective relative permittivity and permeability.[5,6] Such restriction constrains the band expansion based on the superposition of different resonant modes. Despite that the stereo structures can be introduced, some limitations are still there. In the case of the multilayer broadband structure, for example, the resonance of the underneath layer is excited by the penetrating wave from the above layer, so practically the number of the stacking layers cannot be too many to keep a nearly equal strength for the different modes designated to each layer. This limitation becomes even more evident when the electromagnetic loss or mechanical loss becomes more significant.

To achieve a flat plateau in the absorption spectrum, people may introduce gradient structures,[88–102] self-similar fractal structures,[103–115] and disordered structures.[116–119] The gradient structure stands for a type of component in the unit cell that continuously changes the geometrical parameters and hence can support a broadband resonance. One interesting work applying this idea is to design the crossed trapezoidal arrays on a silver film,[90] which realized an ultrathin broadband absorber, as illustrated in **Figure 4**a. In this scenario, the broadband feature arises from the resonant electromagnetic responses of different cross-sections of the trapezoid at different frequencies.[90,91] In addition to the gradient structures with 2D configuration, stereoscopic gradient structures can also be applied, which provide additional freedom in arranging the resonant units. For example, a periodic array of metal–dielectric multilayered quadrangular frustum pyramids has been designed for the broadband metamaterial absorbers (Figure 4b).[92] The width of the structure gradually increases

from the top to the bottom, which can support resonances with different frequencies.[92–100] A similar strategy can be applied to the designing of broadband emitter as well.[101] In addition to the aforementioned gradient resonant structures, the self-similar fractal structure[103] is also capable of embodying different frequencies within a limited space.[104–115] Zhu et al. reported that the quantum efficiency can be significantly enhanced in an ultrathin silicon solar cell coated with a fractal-like pattern of silver nanocuboids (Figure 4c).[106] Due to the coexistence of several feature sizes in the fractal pattern, multiple cavity modes and surface plasmon modes are simultaneously excited. Superimposing those multiple cavity modes and surface plasmon modes eventually contributes to the broadband absorption in the solar cell.[104,106] Furthermore, disordered structures can be applied to increase the bandwidth and efficiency of solar energy harvesting as well.[118,119] An assembly of random-sized plasmonic absorbers[119] has been realized with gold nanoparticles with different size distribution, as shown in Figure 4d, which enables a high density of hybridized localized surface plasmon resonance, and absorbs light in a wide wavelength range from 400 nm to 10 μm.

2.2. Broadband Response Based on Dispersion Compensation

Another efficient approach of expanding the bandwidth is to utilize dispersion compensation in designing the artificially structured material. Such a strategy is necessary in many scenarios. For traditional dielectric material, such as glass, the intrinsic material dispersion[11] leads to longer focal lengths at a lower frequency in a refractive lens, which induces chromatic aberration
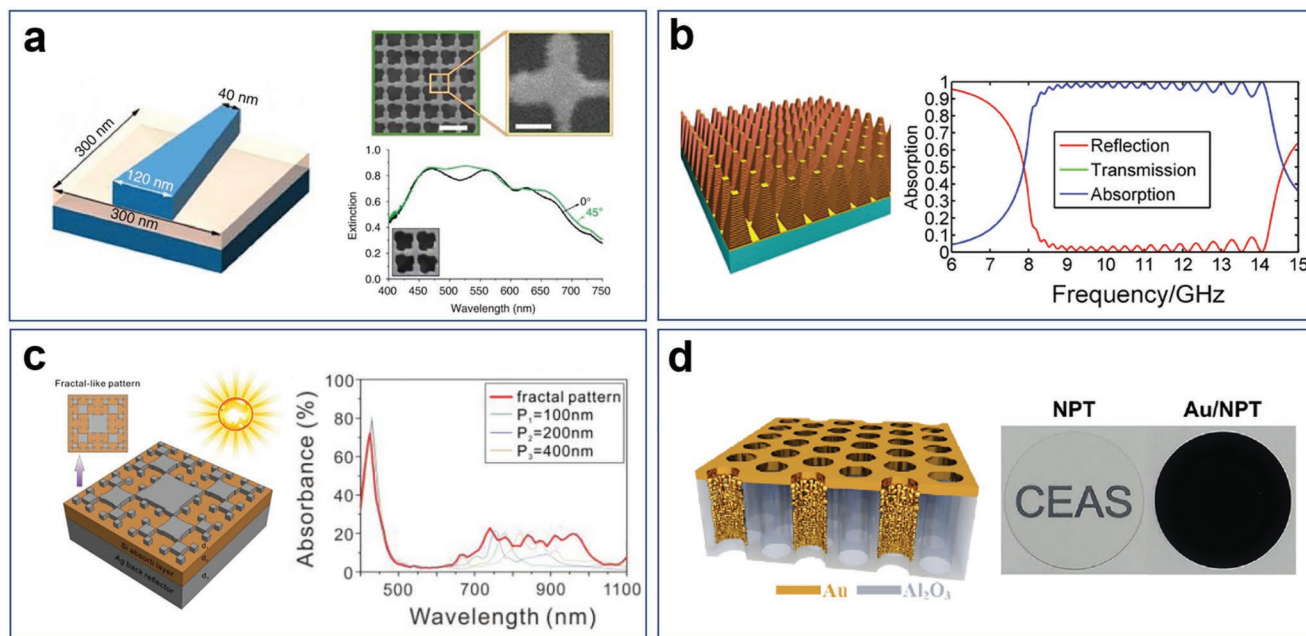
Figure 4. Superimposing different resonant modes to achieve a broadband response. a) The schematics of the single trapezoid unit cell (left panel) and SEM images and the measured extinction spectra of the fabricated crossed trapezoid arrays (right panel). In the SEM images, scale bars are 500 and 100 nm, respectively. Reproduced with permission.[90] Copyright 2011, Springer Nature. b) Broadband absorber made of a periodic array of metal–dielectric multilayered quadrangular frustum pyramids and the simulated reflection, transmission, and absorption spectra. Reproduced with permission.[92] Copyright 2012, AIP Publishing. c) The schematic of the ultrathin silicon solar cell with a fractal feature, and calculated absorbance spectrum of the fractal-featured silicon solar cell (red line). Reproduced with permission.[106] Copyright 2013, Optical Society of America. d) 3D schematic of the self-assembled plasmonic absorbers and the comparison of the transmission between a bare nanoporous template (transparent, left) and a ≲90 nm thick gold-deposited nanoporous template (completely black, right). Reproduced with permission.[119] Copyright 2016, American Association for the Advancement of Science. The Authors, published by American Association for the Advancement of Science (AAAS). Reprinted/adapted from ref. [119]. © The Authors, some rights reserved; exclusive licensee American Association for the Advancement of Science. Distributed under a Creative Commons Attribution NonCommercial License 4.0 (CC BY-NC) http://creativecommons.org/licenses/by-nc/4.0/.

in imaging. For the diffractive optical elements, such as a Fresnel lens, the opposite tendency occurs, and the focal length decreases at the lower frequency. Such a dispersion originates from different phase accumulation through light propagation.[13] In the scenario of artificially structured materials, the excited resonances are also dispersive, which limit the working bandwidth.[16] In this section, we focus on some approaches to reach broadband response with a dispersion compensation strategy.

2.2.1. Dispersion Compensation via the Multiplication of the Contributions from Different Dispersion

The system with dispersion compensation involves two or more types of materials/components. The electromagnetic broadband response of the whole system can be achieved via the multiplication, addition, or subtraction of the contributions from different parts. The detailed physics mechanism varies. Yet the essential strategy is that by elaborately selecting materials and constructing metastructures, certain algebra operation on the contributions from different dispersion components occurs when the electromagnetic wave interacts with the metastructures. Consequently, a dispersion-free effect can appear in the electromagnetic response within a certain frequency range. In 2014, Jiang et al. reported the broadband response based on the dispersion compensation by the multiplication of the contributions from

different dispersion (**Figure 5**a) in the metal–insulator–metal (MIM) structure.[16] Several earlier studies[120–124] have indicated that the broadband effect exists in the MIM structure, yet the underlying mechanism was not elucidated. In ref. [16], Jiang et al. provided a clear physics picture of the MIM design, where the resonant phase dispersion in the metallic structure is compensated by the thickness-dependent dispersion of the dielectric spacing layer. As illustrated in Figure 5b, the light reflected from the lower solid metallic film can be regarded as the radiation of the mirror image of the above metallic metastructure, and hence the overall reflected electric field can be taken as the superposition of each component propagating in the +z direction as

$$\vec{E}_{\text{ref}} = -\vec{E}_{\text{inc}} + \vec{E}_{\text{rad}} \times \left(-e^{ikd} + e^{-ikd} \right) \qquad (1)$$

where $\vec{E}_{\text{ref}}$ originates from the Lorentz resonance of the L-shaped metallic structure, and the term $-e^{ikd} + e^{-ikd}$ stands for the frequency-dependent conjugation between the radiation from the metallic structure and that from its mirror image. In this configuration, the thickness of the dielectric interlayer, d, is the key parameter leading to the frequency independence of the overall dispersion. By changing the dielectric interlayer thickness d, the amplitude of the reflected light shows a complicated function of the frequency. However, when the dielectric interlayer thickness d is selected as a specific value,[16] the amplitude of the irradiation $\vec{E}_{\text{rad}}$ increases with the frequency,
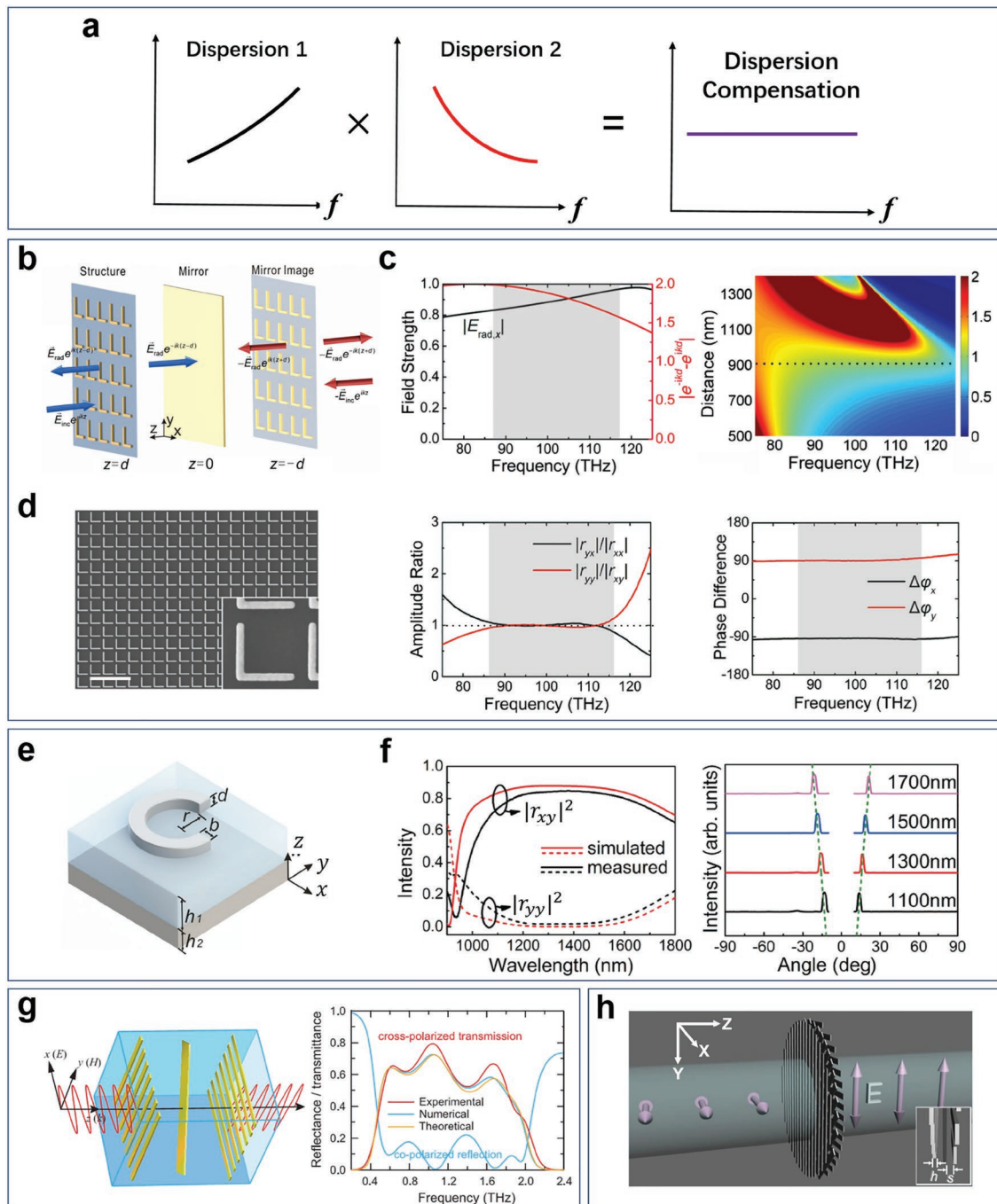
Figure 5. The dispersion compensation via multiplication of the contributions of different components in the metastructure to achieve a broadband response. a) The schematics to show the operation of dispersion compensation via multiplication of the contribution of different components. b) The schematics to show the interaction of light with the array of L patterns ($z = d$) in front of a perfect electric conductor ($z = 0$), the mirror image of the array is located at $z = -d$. c) The left panel shows that as frequency increases, the amplitudes of the x-components of the irradiation of the structure increase, whereas $|-e^{ikd} + e^{-ikd}|$ decreases. The dashed line in the right panel demonstrates that when the interlayer thickness d is selected as 911 nm, the color (amplitude ratio of the x- and y-polarized reflected light) along the dashed line remains a constant across a broad frequency region, indicating the dispersion-free feature at this specific interlayer thickness. d) The SEM image of the array of gold L patterns, the bar represents 5 μm. The middle and right panels are the experimentally measured amplitude ratio and phase difference of the sample under the illumination of x- and y-polarized light, respectively. b–d) Reproduced under the terms of the CC-BY Creative Commons Attribution 3.0 Unported License (http://creativecommons.org/licenses/by/3.0/).[16] Copyright 2014, American Physical Society. e) The plot of a split ring, which serves as the building block of the metasurface. f) The simulated and measured reflectance of the array of the split rings, and the angle-resolved light intensity distribution for the wavelengths of 1100, 1300, 1500, and 1700 nm, respectively. e,f) Reproduced with permission.[128] Copyright 2015, American Physical Society. g) The schematics of the broadband metamaterial linear polarization converter, and the obtained cross-polarized transmittance. Reproduced with permission.[17] Copyright 2013, American Association for the Advancement of Science. h) The schematics of the three-layer grating, working as a tunable polarization rotator for the broadband terahertz waves. Reproduced with permission.[140] Copyright 2015, Wiley-VCH.

**ADVANCED
SCIENCE NEWS**
www.advancedsciencenews.com

**ADVANCED
MATERIALS**
www.advmat.de

whereas the conjugated term $|-e^{ikd} + e^{-ikd}|$ decreases with the frequency (see the left panel of Figure 5c). Interestingly, the increase $\vec{E}_{rad}$ can be compensated by the decrease of the conjugated term $|-e^{ikd} + e^{-ikd}|$ within a broad frequency region by multiplying these two terms. Consequently, the amplitude ratio of the x- and y-polarized reflected light remains the same over a very broad frequency range (see the dashed line in Figure 5c). Both simulated and experimental data (Figure 5d) show that a dispersion-free quarter waveplate is achieved with a bandwidth of about 30% of the central frequency.[16] This approach is a typical example of dispersion compensation via the multiplication of the contributions from different dispersion.

This principle can be extended to other sandwiched MIM nanostructures, such as gold or silver nanorod,[125,126] metallic cut-wire pairs,[127] split rings,[128] and ring/disk cavity.[129] In Figure 5e, the unit cell of a silver split ring with a 45° orientation angle is introduced.[128] By tuning the thickness of the SiO$_2$ spacing layer, the dispersion of the reflected electric field can be compensated, and hence a broadband linear polarization convertor with high efficiency is achieved for near-infrared light (left panel of Figure 5f). It has been known that the nanoantenna with a high polarization conversion ratio is an excellent candidate to generate the Pancharatnam–Berry (PB) phase by rotating the orientation of the antenna while maintaining the other geometrical parameters.[130,131] In this case, when the orientation angle of the split ring rotates along the x-direction, a PB phase gradient is generated. It follows that with a linearly polarized light normally incidence, the metasurface generates two anomalous reflection beams with a high conversion efficiency of more than 70% from 1100 to 1750 nm, as shown in the right panel of Figure 5f.[128] In addition to anomalous reflection, the broadband PB phase based on MIM configuration is also effective for other devices such as holograms[126,132] and metalenses.[133,134] It has been reported that a broadband holographic image can be formed with a circularly polarized light from 630 to 1050 nm.[132]

The application of dispersion compensation via the multiplication of the contributions from the resonant phase dispersion in the metallic structure and the thickness-dependent dispersion of the dielectric spacing layer is not limited to the reflection mode in the MIM structure, it occurs to the transmission mode as well. Grady et al. demonstrated broadband and high-efficiency terahertz polarization converter in transmission mode, as shown in the left panel of Figure 5g.[17] The schematic of the unit cell is similar to the MIM configuration, except replacing the solid metallic ground plane with a metal grating. This grating allows transmission of the cross-polarized waves but reflects the co-polarized wave like a metal ground plane. As validated by both calculations and experiments (Figure 5g), it is capable of rotating a linear polarization state into its orthogonal orientation with high efficiency in the range from 0.52 to 1.82 THz.[17] A broadband polarization rotator can also be made by multilayers with a similar mechanism.[135–141] Fan et al. demonstrated a freely tunable polarization rotator for broadband terahertz waves with a three-rotating-layer metallic grating structure (Figure 5h).[140] By mechanically rotating the orientation angles of three gratings, the polarization of the linearly polarized THz wave can be conveniently rotated to any desired direction with nearly perfect conversion efficiency.

2.2.2. Dispersion Compensation via Adding the Contributions from Different Dispersion

Apart from the multiplication, adding up the contributions from two types of dispersion with the opposite evolution tendency with respect to frequency can also lead to a dispersion-free structure with broadband response, as illustrated in **Figure 6**a. It has been known that the phase discontinuity originated from the PB phase is dispersion-free[142–144]; i.e., the PB phase depends on the orientation angle of the building block only, and it is not related to the other geometrical parameters. However, even for the broadband PB-phase-based metamaterials,[145,146] due to the different phase accumulation through light propagation with different wavelengths, strong chromatic aberration remains, which limits their performance in broadband focusing and imaging.[13] By superimposing multiple independent resonances in a unit cell, achromatic metalens working at several discrete frequencies or narrowband can be achieved.[13,147–149] Recently, Wang et al. employed the integrated-resonant unit element, which consists of basic geometric phase and compensated resonant phase to realize broadband achromatic flat optical components (inset of Figure 6b).[18] When the working wavelength satisfies $\lambda \in \{\lambda_{min}, \lambda_{max}\}$, the distribution of phase retardation for an ideal achromatic metalens can be expressed as the sum of two parts

$$\varphi(R, \lambda) = \varphi(R, \lambda_{max}) + \Delta\varphi(R, \lambda) \tag{2}$$

where

$$\Delta\varphi(R, \lambda) = -\left[2\pi\left(\sqrt{R^2 + F^2} - F\right)\right]\left(\frac{1}{\lambda} - \frac{1}{\lambda_{max}}\right) \tag{3}$$

Here, R is the distance from arbitrary position on the metalens to the center and F is the focal length. The first term in Equation (2) can be easily acquired from the geometric phase, which can be adjusted by changing the orientation angle of the building block. Meanwhile, the second part of Equation (2) (for details in Equation (3)) requires that the phase response be linearly proportional to the wavenumber. One approach to realize such dispersion is to judiciously design the resonance phase response of metallic structures. Because the mechanism of this resonant phase response in this system[18] is completely different from the geometric phase, these two parts of the phase do not interfere with each other. Instead, they can be simply added up. Via this "adding up" operation, the contributions of different components compensate each other, thus forming a dispersion-free region. The simulations in Figure 6b demonstrate that the integrated-resonant unit element can satisfy this requirement. As shown in the gray region of Figure 6b, the conversion efficiency remains nearly a constant when the reflected phase changes linearly with the wavenumber. This indicates that the addition of the contributions from the geometric phase and resonant phase can provide an accurate achromatic phase profile for the metalens within a certain wavelength range. To verify it, an achromatic converging metalens designed for bandwidth from 1200 to 1680 nm has been fabricated (Figure 6c). With a numerical aperture of 0.268, the focal length of the achromatic metalens remains almost a constant for different incident wavelengths. For most optical applications, however,
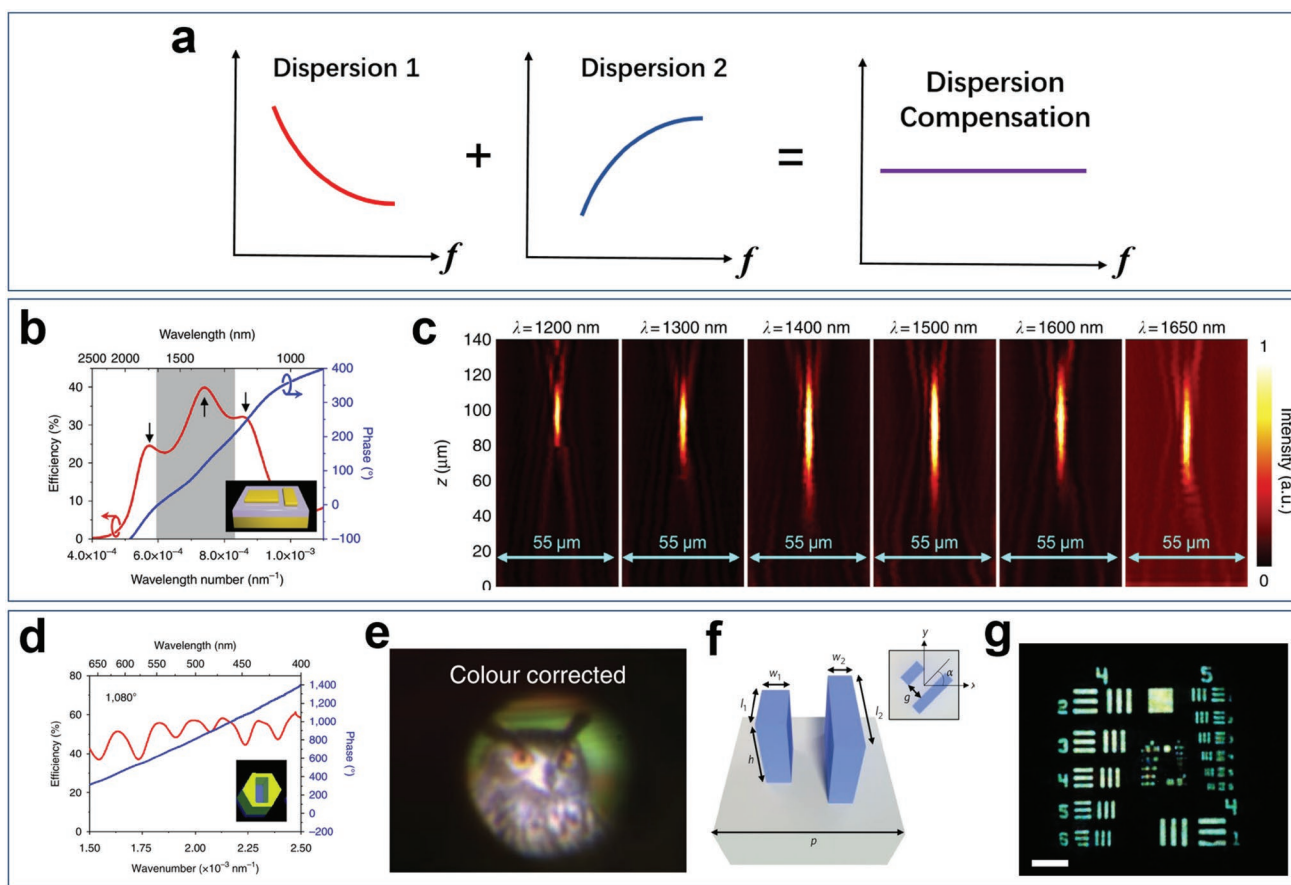
**ADVANCED
SCIENCE NEWS**

www.advancedsciencenews.com

**ADVANCED
MATERIALS**

www.advmat.de

Figure 6. The dispersion compensation based on adding up the contributions of different components to achieve a broadband response. a) The schematics to show the dispersion compensation based on adding up the contributions of different components. b) The efficiency to convert a right-circular-polarized state to left-circular-polarized state (red curves) and phase response (blue curves). c) Experimental intensity profiles of broadband achromatic metalens along axial planes at various incident wavelengths. b,c) Reproduced under the terms of the CC-BY Creative Commons Attribution 4.0 International License (http://creativecommons.org/licenses/by/4.0/).[18] Copyright 2017, The Authors, published by Springer Nature. d) The plot of the circularly polarized conversion efficiency (red curves) and phase response (blue curve) for the integrated-resonant unit element with phase compensation of 1080°. e) The captured images from an achromatic metalens after color correction. d,e) Reproduced with permission.[150] Copyright 2018, Springer Nature. f) The schematic of a metalens element consists of two TiO$_2$ nanofins, which are rotated to the center of the square. g) The achromatic metalens imaging of the standard resolution target with an illumination bandwidth of 200 nm centered at 570 nm. f,g) Reproduced with permission.[151] Copyright 2018, Springer Nature.

transmission schematic is more desirable. Therefore, recently such a design strategy has been applied to a dielectric metasurface, which works in the visible regime with transmission mode.[150,151] Gallium nitride, which is lossless in the visible regime, is applied to build the integrated-resonant unit element (the inset of Figure 6d).[150] The simulations in Figure 6d show that the gallium nitride structure provides a linear relationship between the phase response and the wavenumber. The measurements demonstrate that the focal length of this dielectric achromatic metalens remains a constant for the wavelength between 400 and 660 nm. The full-color imaging with this achromatic metalens indicates that the device is promising for the full-color optical applications (Figure 6e).[150] During the same period, Chen et al. also illustrated that by judicious designing of TiO$_2$ nanofins on a surface, a transmission achromatic metalens with large bandwidth can be achieved (Figure 6f), and white-light achromatic imaging from 470 to 670 nm has been experimentally realized, as shown in Figure 6g.[151]

2.2.3. Dispersion Compensation via the Subtraction of the Contributions of Different Dispersion

The broadband response can also be realized by using dispersion compensation via the subtraction of the contributions of the different components (**Figure 7**a). The idea was theoretically and experimentally demonstrated by Wu et al. with a metallic helix array (Figure 7b).[152] In the earlier studies, due to the specific asymmetric shape, helix array has been extensively investigated as a chiral metamaterial.[153–159] By choosing certain geometrical parameters to control the local resonance of nanostructures and Bragg scattering of periodic structures, Wu et al. demonstrated that the dispersion relation for the right- and left-handed elliptically polarized eigenstates can be simultaneously modulated.[152] The calculated band structure in Figure 7c shows that for a specific design, the dispersion of the lowest branch B_R (black solid line, the degenerated ±1 orders of helical Bloch states with the electric fields along the
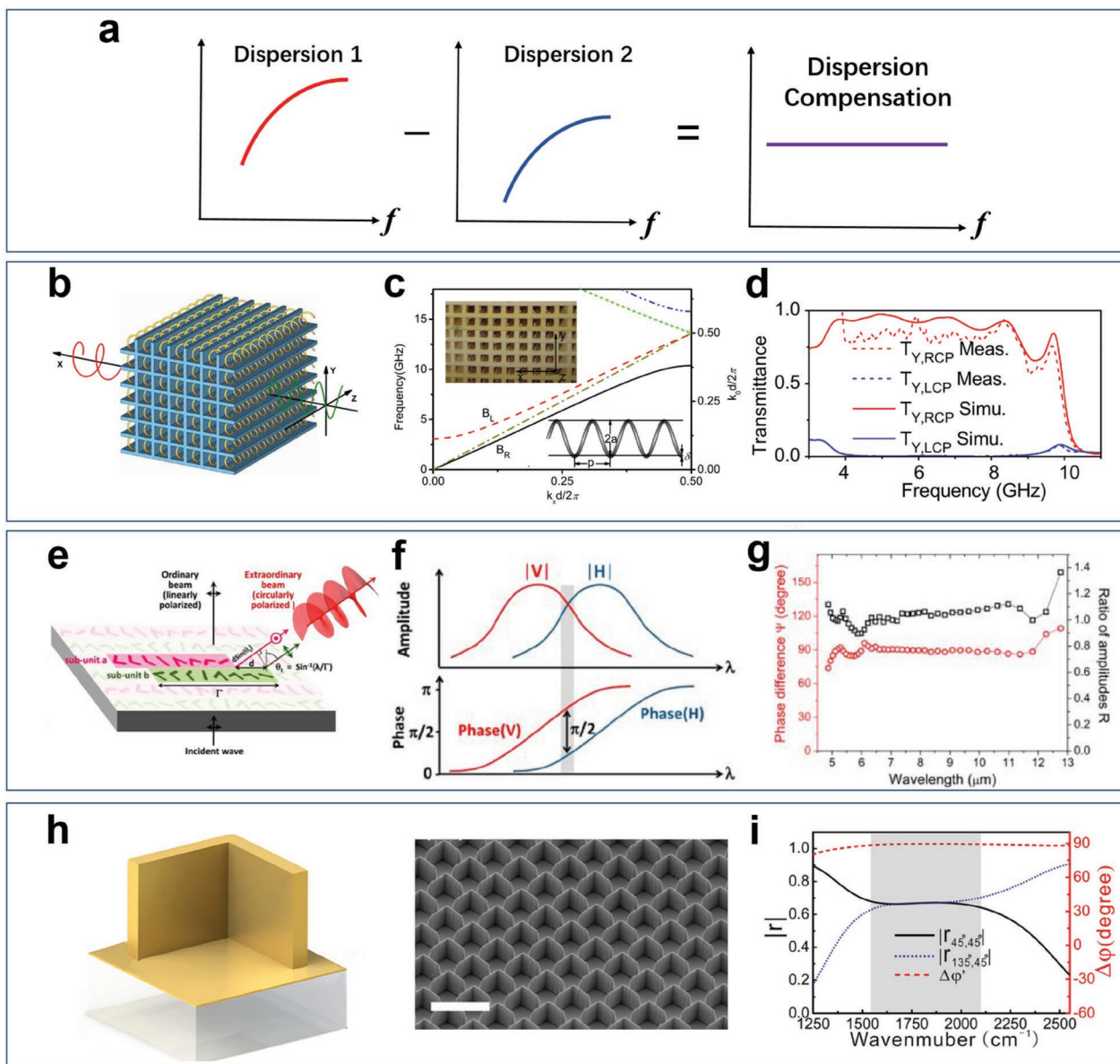
Figure 7. The schematics of the approaches to realize the broadband response by dispersion compensation via subtracting the contributions of the components. a) The schematics of dispersion compensation via subtraction of the contributions of different components. b) The schematics to show the transverse propagation through the array of helices, which are arranged in a square lattice. c) The experimental realization of the designing in (b) and the corresponding dispersion diagram. d) The plot shows both the calculated and measured transmission spectra of the helix array. b–d) Reproduced with permission.[152] Copyright 2011, American Physical Society. e) The plot to show the designing of the unit cell consisting of two subunits, each with eight gold V-shaped antennas. f) The schematics to show that two orthogonal plasmonic eigenmodes, V and H (red and blue curves), can be excited by an array of identical anisotropic plasmonic structures. g) The calculated phase difference Ψ and the ratio of amplitudes R of the two orthogonal waves. e–g) Reproduced with permission.[161] Copyright 2012, American Chemical Society. h) The schematics of the designed L-shaped stereo structures (LSSs) unit, and the SEM image of the LSS array. The scale bar represents 5 µm. i) The calculated amplitudes of the reflected light and the phase difference for different polarizations. h,i) Reproduced under the terms of the CC-BY Creative Commons Attribution 3.0 Unported License (https://creativecommons.org/licenses/by/3.0/).[164] Copyright 2014, The Authors, published by AIP Publishing.

y-direction) and the second-lowest branch B_L (red dashed line, the zeroth order of helical Bloch state with the electric fields along the z-direction) are almost linear and parallel each other in a broadband range. In this case, two orthogonal eigenstates of the B_R and B_L branches pick up the same phase difference in a wide frequency range. This broadband mechanism is quite different from previous ones that utilize helix structures like that

in ref. [153], where light propagates along the helix axis and the broadband response originates from the superposition of three standing wave modes along the propagation direction, as discussed in Section 2.1. In the scenario of ref. [153], the metastructure can only block the circular polarization with the same handedness as the helices and work as a broadband circular polarizer. However, dispersion compensation via the subtraction

of the contributions of the different components can realize more functions in broadband waveplates. This unique design has been experimentally demonstrated, as shown in Figure 7d, where the γ-polarized light transmits through the helical array and turns into the right-handed circular polarized light. The bandwidth ranges from 3.9 to 9.6 GHz, as schematically illustrated in Figure 7d. The experimentally measured transmission spectra are in good agreement with the simulations. Based on the same dispersion–compensation principle, more nanostructures supporting two orthogonal resonant modes with a constant phase difference have been reported.[160–167] Yu et al. proposed a metasurface to realize broadband polarization conversion with high efficiency in the mid-infrared regime.[161] The unit cell consists of two spatial separated subunits (the pink and the green ones in Figure 7e), generating two co-propagating waves with equal amplitudes and orthogonal polarizations. The phase difference between these two co-propagating waves is fixed at $\pi/2$ over a large frequency range, as shown in Figure 7f. Via coherent interference, this metasurface acts as a quarter waveplate and generates a circularly polarized beam. The measured phase difference Ψ and amplitude ratio R in Figure 7g indicate that Ψ and R are very close to 90° and 1, respectively, suggesting that a broadband quarter waveplate has been realized in the wavelength ranging from 5 to 12 μm.[161] Instead of introducing volumetric metamaterials or combining two subunits inside one unit cell, Xiong et al.[164] introduced a new broadband approach, which consists of standing metallic L-shaped stereo structures (LSSs), as shown in Figure 7h. Each arm excites one electric dipole and builds the desired dispersion as shown in Figure 7f. The reflected spectra and phase response are simulated in Figure 7i. When the incident light is 45°-polarized, the reflected amplitudes for 45°- and 145°-polarized light are almost identical in the range of 1550–2100 cm^{-1}, and the phase difference between 45°- and 145°-polarized light remains 90°. This situation means that a right-circular-polarized light has been realized within this frequency range.

2.3. Broadband Response Based on the Nonresonant Effects of the Metastructures

As discussed in previous sections, the broadband response can be achieved via superimposing multiple resonant modes or by dispersion compensation. An alternative approach to realize the dispersion-free effect is to use the nonresonant feature of some metastructures, where the dispersion spectrum becomes nearly flat. Three different ways to realize the broadband response are presented in this section: using the nonresonant response of nondispersive materials; selecting a working frequency far away from the resonant frequency of the structure, and relying on the frequency-independent physical effects to realize the broadband electromagnetic response.

2.3.1. The Nonresonant Response of Nondispersive or Low Dispersive Materials

The broadband response can be achieved by using the nonresonant feature of the nondispersive or low-dispersion meta-

materials (**Figure 8**a). Because most dielectric materials are low dispersive in a certain frequency range, people can take the advantage of this feature to design the broadband materials, which has been successfully applied in broadband cloaking,[168–171] lenses,[172–175] antennas,[176] photonic crystals,[177,178] etc. For example, Ma et al.[172] presented a 3D broadband flattened Luneburg lens made of nonresonant metamaterial, which is fabricated by drilling inhomogeneous holes on the multilayered dielectric plates. The continuous variation of the refractive index (n) has been realized by tuning the air filling ratio by changing the diameter (D) of the holes in the unit cell (Figure 8b). It has been reported that some 2D materials also have low-dispersion features, which are good candidates to fabricate ultrathin broadband metamaterials. As illustrated in Figure 8c, at the frequency lower than $2E_F/h$ (where E_F is the Fermi energy), such as in the terahertz frequencies, the sheet conductance of monolayer graphene is dominated by intraband transitions and exhibits a value of $(e^2 E_F \tau)/(\pi \hbar^2)$.[179] This conductance can lead to broadband absorption. Moreover, by controlling Fermi energy E_F with electrical gating or chemical doping, this broadband absorption is also tunable.[179] Based on the broadband and tunable properties of conductance, monolayer or a few layers of graphene can be employed to design the broadband electro-optic modulators.[179–188] For example, Liu et al.[180] experimentally demonstrated a broadband, high-speed, and waveguide-integrated electroabsorption modulator based on monolayer graphene (Figure 8d). By electrically tuning the Fermi level of the graphene sheet, they experimentally demonstrated a broadband modulator operating in the range from 1.35 to 1.6 μm, with the operation speed higher than 1.0 GHz.[180] Besides, terahertz modulators with high tunability in both intensity and phase are essential for effective control of the electromagnetic properties. Chen et al.[187] demonstrated a highly tunable solid-state graphene/quartz modulator based on the low-dispersion sheet conductance of graphene (left panel in Figure 8e). By controlling the electric gate, the conductivity of the graphene can be varied and hence the refractive index can be tuned. In this way, a nearly perfect intensity modulation with the modulation depth (the ratio of reflection change to original reflection) higher than 99.3% from 0.5 to 1.6 THz (middle panel in Figure 8e) has been achieved. Meanwhile, the relative phase shift of the reflected light remains more than 140 degrees in this broadband range (right panel in Figure 8e).[187]

2.3.2. Selecting Working Frequencies Far Away from the Resonances in the Metastructures

Another approach to realize the dispersion-free feature is to select a working frequency far away from the resonant point. This type of metamaterials is usually termed as nonresonant metamaterials.[19] The dispersion of nonresonant metamaterials is nearly flat, and the permittivity and permeability do not significantly vary with the frequency of the incident light (**Figure 9**a). This scenario is very similar to that of the dielectric material, and the interaction with the electromagnetic waves is much weaker, which can decrease the absorption of the incident light. Utilizing the metal-based nonresonant metamaterial elements, Liu et al. found out that the permittivity in the zero-frequency
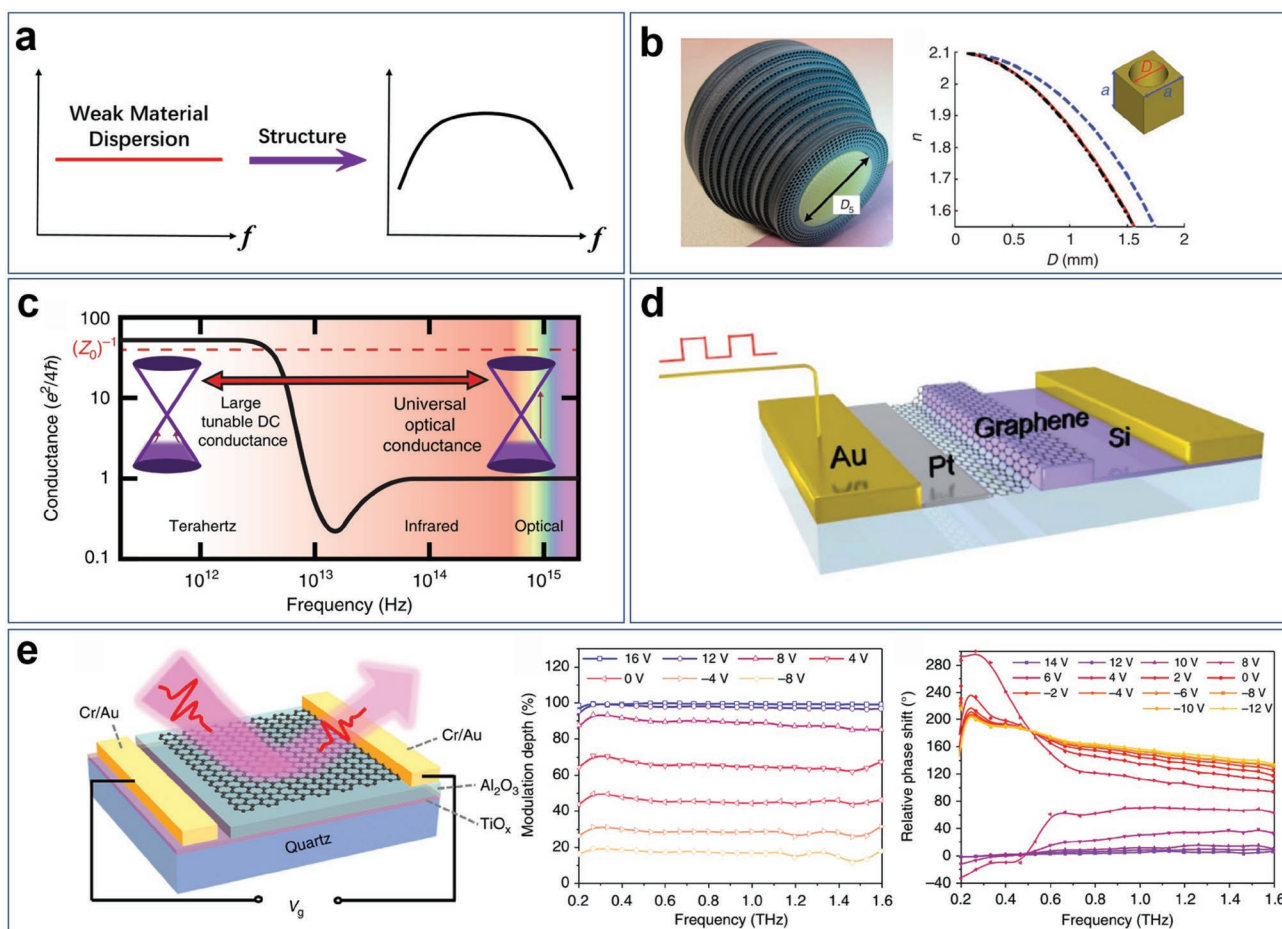
Figure 8. The broadband response based on non-dispersive materials. a) The schematics of the broadband response based on nondispersive materials. b) The photograph of a 3D flattened Luneburg lens (left), and the relationship between the refractive index and the hole's diameter of the unit cells (right). Reproduced with permission.[172] Copyright 2010, Springer Nature. c) The qualitative trend of the frequency-dependent conductance for monolayer graphene normalized to $e^2/4\hbar$. The optical frequency range exhibits a universal value of 1, whereas in the THz range, the conductance can be orders of magnitude higher. Reproduced under the terms of the CC-BY Creative Commons Attribution 4.0 International License (http://creativecommons.org/licenses/by/4.0/).[179] Copyright 2017, The Authors, published by Springer Nature. d) The schematics of a graphene-based broadband optical modulator. Reproduced with permission.[180] Copyright 2011, Springer Nature. e) The plot to show the 3D diagram of the graphene-controlled device for ultra-broadband terahertz modulation (left). The modulation depth (middle) and relative phase shift (right) are shown as a function of frequency. Reproduced under the terms of the CC-BY Creative Commons Attribution 4.0 International License (http://creativecommons.org/licenses/by/4.0/).[187] Copyright 2018, The Authors, published by Springer Nature.

limit (the working frequency far away from the resonant frequency) can be expressed as

$$\varepsilon(\omega \to 0) = 1 + \frac{f_p^2}{f_0^2} \tag{4}$$

where f_p is the plasma frequency and f_0 is the resonant frequency of the metamaterial elements.[19] It follows that the permittivity of the nonresonant metamaterials in the zero-frequency limit can be tuned by changing the geometry of the metamaterial element (i.e., changing the resonant frequency f_0) (Figure 9b).[19] Such nonresonant metamaterials can be applied to facilitate many devices, such as broadband cloaking structures,[189–199] lenses,[19,200–206] antennas,[207–220] and other broadband metamaterials.[221–224] The ground-plane cloaking, for example, provides the cloaked objects an appearance of a flat conducting sheet. Since the resonance point of the structure has been avoided, the

electromagnetic loss is no longer a significant issue. Based on this principle, Liu et al. experimentally realized a ground-plane cloaking (Figure 9c). To match the complex spatial distribution of the required constitutive parameters, they constructed a metamaterial consisting of thousands of elements with different geometrical parameters, which are determined by an automated design process. These elements possess nonresonant features, resulting in a broad bandwidth (13–16 GHz) for a ground-plane cloak.[189] The other example is the broadband flat metalens made by Kundtz and Smith.[201] The required refractive index profile of the lens is achieved through patterning specific copper strips on a dielectric substrate. The copper strips act as polarizable inclusions in the medium, determining the overall polarizability of the unit cell (Figure 9d). These strips do not resonate in the broad operation frequency range (7–15 GHz).

Another application of the nonresonant metastructures is to achieve broadband negative refraction based on hyperbolic
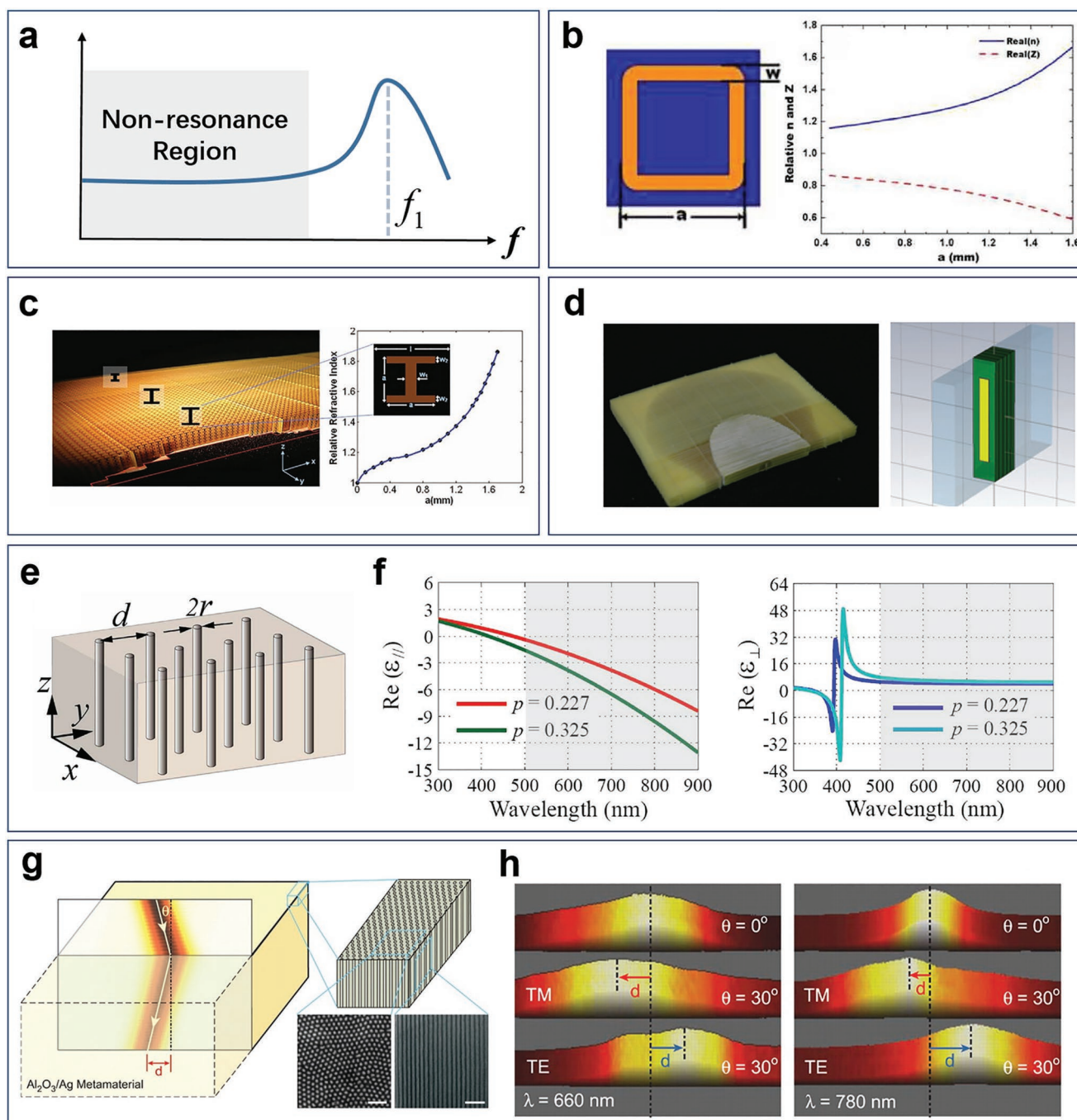
Figure 9. The broadband response realized by selecting the working frequency far away from the resonant region. a) The schematic shows the frequency range with a broadband response, which is far away from the resonant region. b) At frequencies well below the resonance, the unit cell behaves like an effective medium. By changing the unit scale *a* of the metamaterial element, one can tune the value of low-frequency permittivity. b) Reproduced with permission.[19] Copyright 2009, Optical Society of America. c) The photograph of the broadband ground-plane cloaking, the nonresonant elements and the relation between the unit cell geometry (*a* varies from 0 to 1.7 mm) and the effective index. Reproduced with permission.[189] Copyright 2009, American Association for the Advancement of Science. d) The schematic of the flattened Luneburg lens. The required refractive index profile of the lens is achieved by patterning the specific copper strips on a dielectric substrate. Reproduced with permission.[201] Copyright 2010, Springer Nature. e) Schematic of metallic nanowires embedded in a dielectric matrix, constructing the hyperbolic metamaterials. f) The effective permittivities parallel and perpendicular to the nanowire for silver nanowires embedded in an alumina matrix with two different filling ratios. The gray region is far away from the localized SPPs around 400 nm and the property of negative refraction maintains in this area. e,f) Reproduced with permission.[228] Copyright 2008, Optical Society of America. g) The schematic of negative refraction from air into the hyperbolic metamaterials. The zoom-in pictures show the top and side views of the silver nanowires and alumina matrix. The scale bars indicate 500 nm. h) The Measured beam intensity at the existing surface of the metamaterial slab at the wavelength of 660 and 780 nm, respectively. g,h) Reproduced with permission.[229] Copyright 2008, American Association for the Advancement of Science.

metamaterials (HMMs).[225–233] HMMs are a class of highly anisotropic metamaterials that hold hyperbolic dispersion.[225–227] One kind of hyperbolic structures is a large number of metallic nanowires embedded in a dielectric medium, as shown in Figure 9e.[228] In 2008, Liu et al. theoretically demonstrated that by introducing silver nanowires embedded in an alumina matrix, the real part of effective permittivity parallel ($\varepsilon_{\parallel}$) and perpendicular ($\varepsilon_{\perp}$) to the nanowire becomes negative and positive, respectively.[228] In this configuration, as simulated in Figure 9f, the critical condition $\varepsilon_{\parallel} \cdot \varepsilon_{\perp} < 0$ for the negative refraction can be realized in a broad spectral region, as indicated by the gray region, which is far away from the localized surface plasmon polaritons (SPPs) around 400 nm. Thereafter, this idea was experimentally verified by the same group in the silver nanowire metamaterials.[229] Figure 9g illustrates the schematic of the negative refraction from air into the hyperbolic metamaterials. The measured beam intensity shown in Figure 9h demonstrates that the negative refraction occurs in a wide spectral range from 660 to 780 nm.

2.3.3. Relying on the Frequency-Independent Physical Effects

By relying on some frequency-independent physical effects, it is possible to achieve a broadband electromagnetic response in metastructures. Here, we take examples to illustrate that the radiation of surface plasmons, which is frequency independent, can make the structured metals ultra-broadband transparent. It has been found that surface plasmons (SPs) or spoof surface plasmons (SSPs) on the surface of structured metals can lead to extraordinary optical transmission.[1,234] However, due to the underlying resonance mechanisms of the metal, these transparency phenomena occur only in a very narrow frequency band. In 2000, Huang et al.[235] initially predicted that metallic gratings consisting of narrow slits can become transparent for extremely broad bandwidth at oblique incidence (**Figure 10**a). This unique phenomenon of ultra-broadband transparency originates from the radiation of SPs (or SPPs),[235] which is frequency independent. Physically, when the transverse-magnetic (TM) polarized light illuminates the subwavelength metal grating, the incident wave drives free electrons on the conducting surfaces and part of the slit walls to form SPs (or SSPs). The SPs (or SSPs) then propagate on the slit walls but are abruptly discontinued by the bottom edges to form oscillating charges that emit the transmitted wave, which eventually makes those structured metals highly transparent.[235] The corresponding microscopic process is not sensitive to the frequencies of the incident waves, thus leading to ultra-broadband flat transmission. Later on, this effect has been experimentally verified in terahertz (Figure 10b),[236] microwave,[237] and visible[238] regimes. Interestingly, this ultra-broadband transparency of metal gratings can also be macroscopically interpreted by the anomalous impedance-matching mechanism[239] (Figure 10c). Actually as a nonresonant effect, this unusual broadband transparency phenomenon has been verified at wide spectral range,[240–248] and extended from one dimension to two dimensions,[238,249–252] and even generalized from light waves to acoustic waves,[253,254] which achieves promising applications on transparent conducting panels and high-efficiency photovoltaic devices.

There are some other frequency-independent effects that can lead to a broadband electromagnetic response. For example,

enhancing and funneling light efficiently through deep subwavelength apertures are essential in harnessing light–matter interaction. Subramania et al.[255] presented a paradigm structure comprising periodically connected rectangular apertures with two different sizes (Figure 10d). It shows an efficient ultra-broadband funneling of optical power confined in an area as small as $(\lambda/500)^2$, where the optical fields are drastically enhanced.[255–257] This nonresonant effect originates from a frequency-independent quasi-static process, wherein the electrons in the metal respond nearly instantaneously to the incident field and the charges build up across the gaps (see the left panel of Figure 10d). The electric field in each respective slit region has no phase difference; thus, broadband funneling of light is realized via ultra-subwavelength channels beyond resonant platforms. Another example is about a long-standing desire to design a broadband angle-selective system, where only the light with a certain incident angle can go through. Shen et al.[178] utilized a 1D photonic crystal, where two different materials are alternately stacked, to realize the narrow-angle selectivity over a broad frequency range. Due to the impedance match between the sample and the surrounding colorless liquid, the angle-sensitive mode can be preserved over the entire visible spectrum (Figure 10e). All these frequency-independent physical effects are nonresonant ones, which can reduce dramatically the electromagnetic loss of the material. Therefore, the device efficiency in this scenario has been increased, as that reported in the high-performance solar cells,[258] broadband detectors,[259,260] and broadband angular momentum multiplexing.[261]

2.4. The Other Approaches towards Broadband Response

As we indicated in previous sections, currently the broadband response can be realized either by superimposing multiple resonant modes, or via dispersion compensation, or by using the nonresonant effect in the artificially structured materials. Actually, there are some additional ways to achieve the broadband feature.

2.4.1. Expand the Bandwidth by Lowering the Q Factor in a Resonant System

For the resonance of a structure, a dimensionless factor, Q, is usually introduced to designate the relationship between the central frequency f_0 and the FWHM $\Delta f = f_{max} - f_{min}$, which is defined as

$$Q = \frac{f_0}{\Delta f} = \frac{f_0}{f_{max} - f_{min}} \tag{5}$$

By lowering the Q factor of a system at the fixed resonant frequency, the bandwidth of the system $\Delta f = f_0/Q$ increases accordingly (**Figure 11**a). It is known that both the split-ring resonator (SRR) and the electrically coupled LC resonator (ELC) are essentially RLC resonators,[2,262] and the Q factor can be expressed as

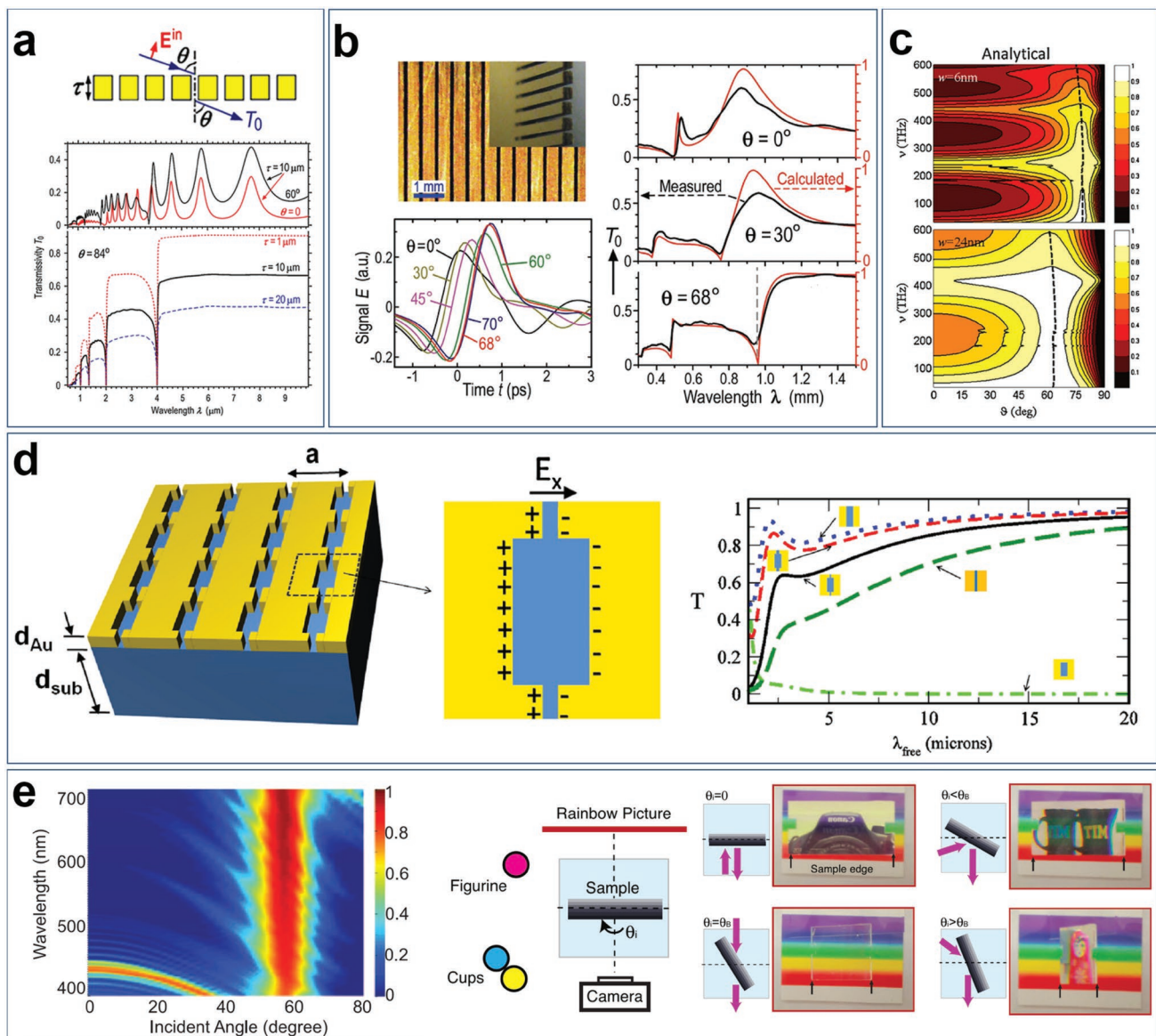$$Q = \frac{1}{R}\sqrt{\frac{L}{C}} \tag{6}$$

Figure 10. The broadband response based on the nonresonant physical effect of metastructured materials. a) The calculated transmission spectra of a gold grating for TM polarization. Reproduced with permission.[235] Copyright 2010, American Physical Society. b) The measurements of TM polarization light transmission through a gold grating. Time-domain THz transmission signals (left panel) and the corresponding transmission spectra (right panel) for different incident angles. The calculated results agree well with the experiments. Reproduced with permission.[236] Copyright 2012, Wiley-VCH. c) The angular transmission spectra for gratings with different widths. The dashed line indicates the anomalous impedance-matching condition. Reproduced with permission.[239] Copyright 2011, American Physical Society. d) A paradigm structure with periodic connected rectangular apertures of two different sizes operating at normal incidence. The schematic depicts the frequency-independent quasi-static process of the charge response. The corresponding transmission spectra are shown in the right panel. Reproduced with permission.[255] Copyright 2011, American Physical Society. e) Experimentally measured p-polarized transmission spectrum. The experimental results in the right panel demonstrate that the sample is transparent (up to 98%) to p-polarized incident light at a critical angle (55°) and behaves like a mirror at all other incident angles over the entire visible spectrum. Reproduced with permission.[178] Copyright 2014, American Association for the Advancement of Science.

where R is the electric resistance, L is the inductance, and C is the capacitance. The resonant frequency is determined by

$$f_0 = \frac{1}{2\pi} \sqrt{LC} \qquad (7)$$

indicating that once L and C are determined, the resonant frequency f_0 remains a constant. Meanwhile, R can be used

as a control parameter to tune the Q factor. The increase of R yields a flatter resonance curve and the decrease of Q factor, whereas a decrease of R yields a sharper resonance curve and the increase of Q factor. Gu et al.[262] reported the expansion of the bandwidth by adding resistors in the metamaterial absorber (with fixed L and C, so f_0 remains a constant). It follows that according to Equation (6), Q factor of this metamaterial absorber decreases; hence, the bandwidth Δf expands (Figure 11b).[262]

**ADVANCED
SCIENCE NEWS**

www.advancedsciencenews.com
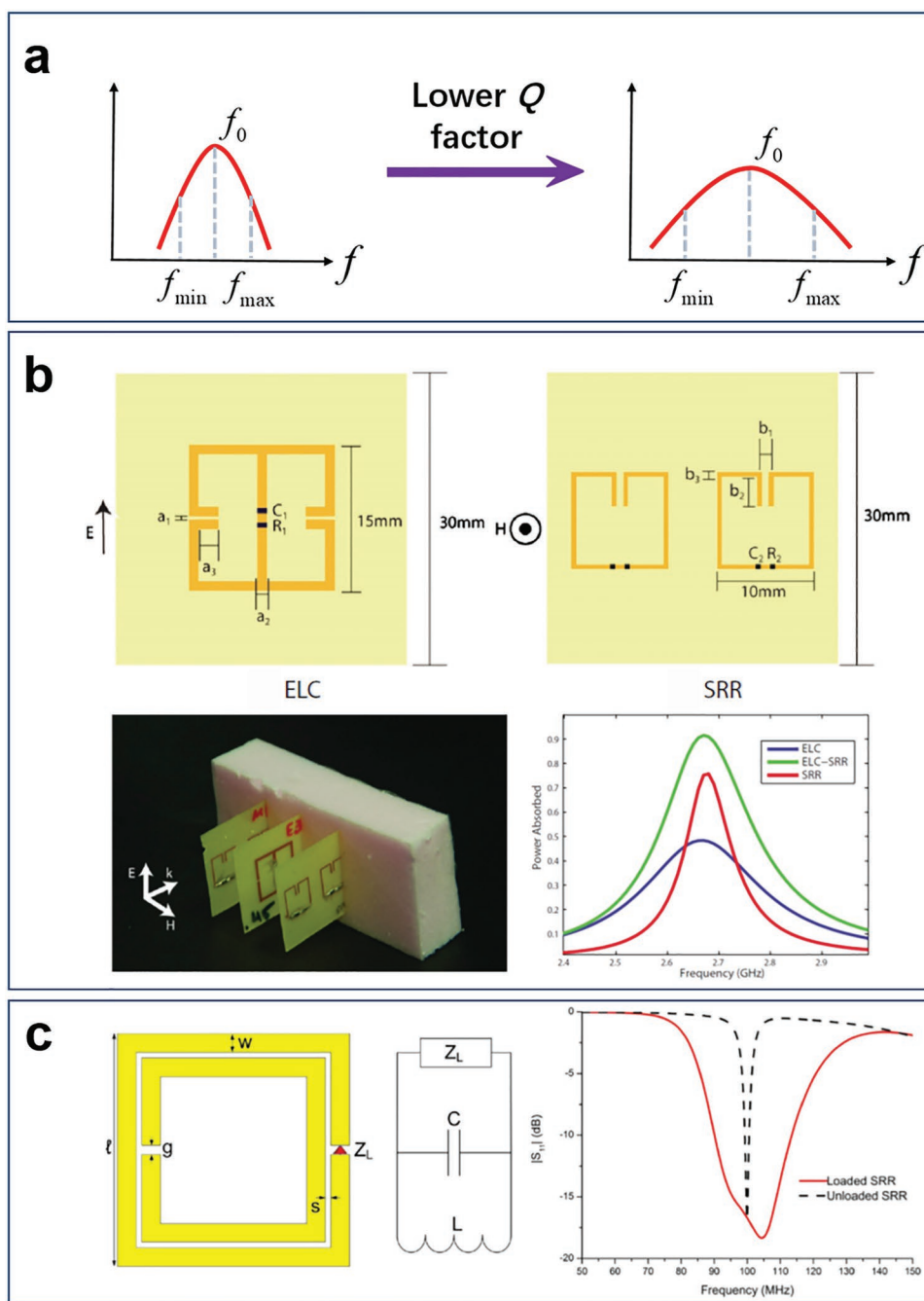
**ADVANCED
MATERIALS**

www.advmat.de

Figure 11. Expanding the bandwidth of a resonant system by lowering the Q factor. a) The schematics to show the expanding of the bandwidth by lowering the Q factor of a resonant system. b) The plot to show the unit cell of an ELC and an SRR structure, the photo of the ELC–SRR absorber, and the simulated absorption of separate and combined ELC–SRR performance. b) Reproduced with permission.[262] Copyright 2010, AIP Publishing. c) The geometry of an SRR loaded with an arbitrary impedance Z_L and its lumped element equivalent circuit representation, and the magnitude of the parameter of the unloaded (dashed line) and loaded (solid line) SRR-based antenna. Reproduced with permission.[266] Copyright 2013, IEEE.

The application of this strategy can be found in exploring new broadband metamaterial absorbers,[262–265] and some other metamaterial-inspired components.[266] The different bandwidth of the unloaded components (without adding extra resistance R or impedance Z_L) and the loaded components (with extra resistance R or impedance Z_L) can be clearly seen in Figure 11c; clearly, the loaded SRR-based antenna (solid line) has a broadened bandwidth comparing with that of the unloaded (dashed line) one.[266]

2.4.2. The Broadband Features in Ultrafast Systems

Another example of broadband response comes from the ultrafast optics, where the duration of the ultrafast optical pulse corresponds to a broadband frequency range after the Fourier transformation (**Figure 12**a). It has been known that for the application of terahertz technology, one of the challenges is to find efficient and compact terahertz emitters/detectors with a
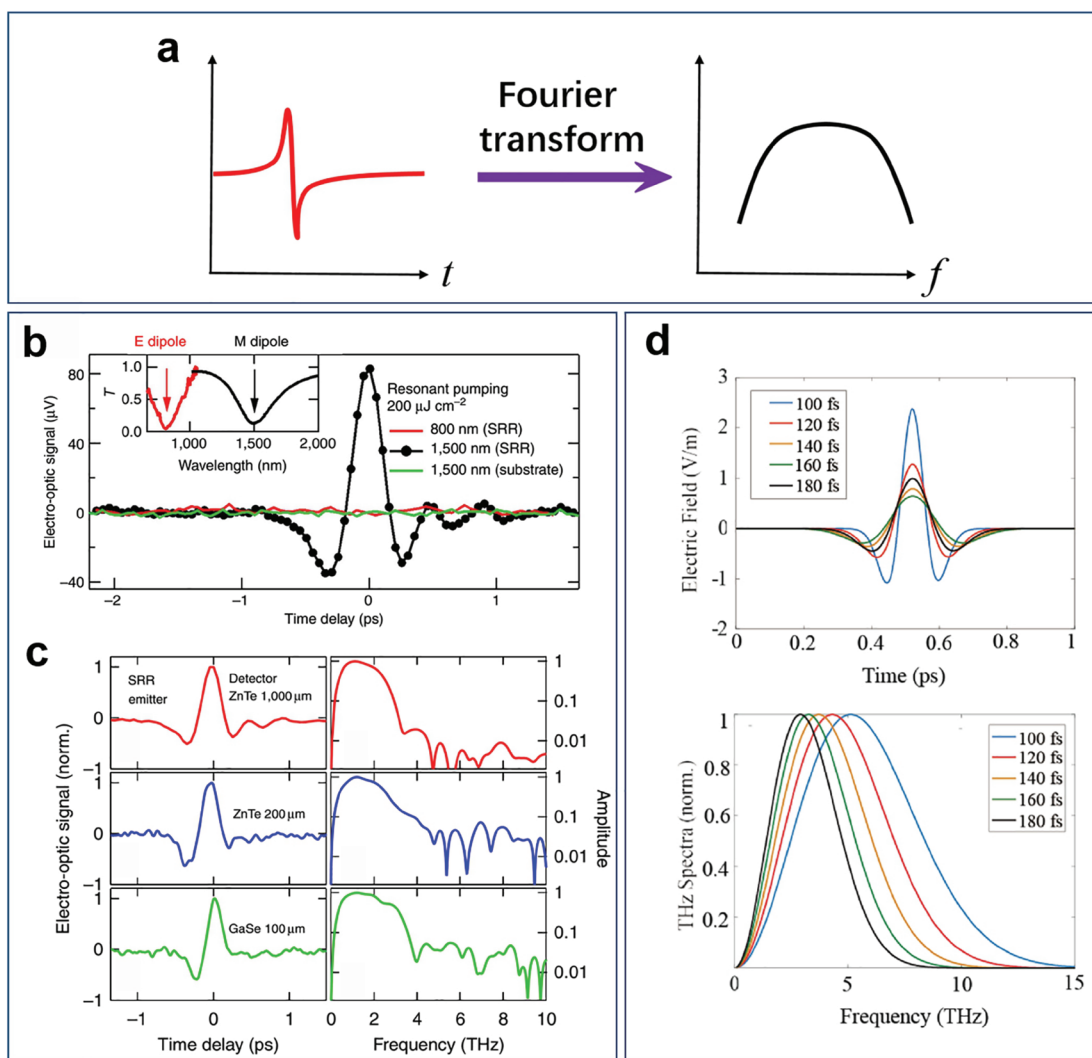
**ADVANCED
SCIENCE NEWS**

www.advancedsciencenews.com

**ADVANCED
MATERIALS**

www.advmat.de

Figure 12. Achieving the broadband response by using ultrafast incident pulses. a) The schematics to show the broadband response based on ultrafast pulses in time. b) The measured THz time-domain signals by pumping the SRR magnetic-dipole resonance (black dots) at 1500 nm; the inset exhibits the linear optical transmission showing electric (red curve) and magnetic (black curve) resonances of SRRs. c) The normalized time-domain THz pulses and the corresponding spectral amplitudes generated from the SRR emitter and three different detectors. b,c) Reproduced with permission.[267] Copyright 2014, Springer Nature. d) The THz pulse traces (100–180 fs) and the corresponding normalized spectral amplitudes. Reproduced with permission.[268] Copyright 2018, Optical Society of America.

broadband spectrum.[267–269] Luo et al.[267] demonstrated an efficient single-cycle broadband terahertz generator in the range of 0.1–4.0 THz, which is composed of a thin layer of split-ring resonators a few tens of nanometers in thickness pumping at the telecommunication wavelength of 1.5 μm (200 THz). The broadband terahertz emission arises from the excitation of a magnetic-dipole resonance in the split-ring resonators (Figure 12b). The bandwidth of the SRR emitter can be as wide as 4.0 THz (Figure 12c). By introducing shorter pumping pulses, even wider terahertz bandwidth can be achieved. For example, the bandwidth of the generated terahertz spectrum can be tuned by changing the duration of the incident Gaussian pulse.[268] The terahertz emission bandwidth and central frequency scale linearly with the bandwidth of the pumping pulse; a shorter pumping pulse of 100 fs leads to a broader terahertz

emission bandwidth comparing to a longer pumping pulse of 180 fs (Figure 12d).[268]

3. Conclusions and Outlook

In previous sections, we briefly summarized the different approaches in designing broadband optoelectric artificially structured materials. The most straightforward strategy in realizing the broadband electromagnetic functionality is to superimpose multiple resonant modes. Despite its wide applications in electromagnetic absorbers, solar cells, antennas, filters, invisibility cloaks, and slow light materials, it indeed possesses some restrictions. Actually to design the metastructures with different independent resonant modes in a limited space

is technically challenging, and to keep those resonant modes non-interferential and equal intensity is also demanding. Therefore, practically it is not easy to combine too many separated resonant modes in a single metastructure.

With nonresonant effects, we can achieve a broadband response, where both the permittivity and the permeability are insensitive to the change of frequencies of the electromagnetic waves. However, due to the nonresonant characteristics of the metastructure, the interaction between light and material is weak. This means that in order to change the states of light, a sufficiently long optical path has to be accumulated. So, the size of the device will not be small, which is not favorable in the trend of device miniaturization and integration.

By tuning the Q factor of a resonating system, it is possible to change the bandwidth with the trade-off of the sensitivity of the system response. Similarly, in the ultrafast optical system, by tuning the pulse duration, the bandwidth can be tuned. In this scenario, however, nonlinearity is usually required to generate the broadband effect,[267] which induces the additional requirements in structural design.

The dispersion compensation approach, among the aforementioned methods in the above sections, seems to be a more elegant strategy. It allows us to manipulate the electromagnetic contributions coming from different dispersion in the structure with certain algebra operation, eventually realizing a frequency-insensitive electromagnetic response. What makes this approach even more interesting is that it usually requires us to combine an artificially structured metallic material and dielectric material. Meanwhile, the strong phase dispersion in the thin metallic structure can be compensated by the thickness-dependent dispersion of the dielectric material. Hence, a dispersion-free feature can be eventually realized. Introducing the hybrid metallic–dielectric metastructures also helps to shrink the device size, which is a very important issue in nanophotonics.

Despite the success so far in developing functional structures with broadband features with different strategies, there are still some aspects awaiting further exploration. One valuable prospect is to achieve broadband electromagnetic multifunctionalities by manipulating multiple degrees of freedom (DOFs) of light (e.g., polarization, amplitude, incident angle, etc.).[270] For example, polarization is a convenient DOF making the broadband electromagnetic functionality, yet most broadband function works only on certain polarization of incident light.[271,272] Recently, by employing meta-units with fourfold symmetry or rotational symmetry, a broadband achromatic polarization-insensitive metalens can be realized, which is highly desirable for compact imaging systems particularly in virtual/augmented reality.[273,274] Furthermore, by tuning more DOFs, several broadband electromagnetic functionalities can be integrated into a single device. For example, one device could act as a broadband hologram, broadband waveplate, and broadband detector/sensor, respectively, by merely changing the incident angle. Such kind of approaches could be further employed to implement more functionalities, including the encryption in information processing. In principle, broadband multifunctional metastructures can build hybrid DOF multiplexing systems, which can be applied for high-density data encoding, security encryption, and optical information engineering.

Another possible hot spot for the future development of metastructures is the active control[275–277] of the bandwidth of metamaterial with external fields, such as electrical field, magnetic field, light field, thermal field, mechanical force field, etc. For many transition metal oxides, the insulator–metal transition occurs due to the microscopic interactions among the charge, lattice, orbital, and spin degrees of freedom. Liu et al. reported an interesting observation of an insulator–metal transition induced by a terahertz electric field in vanadium dioxide, which is covered by gold metastructures.[278] By applying picosecond, high-field terahertz pulses, the Coulomb-induced potential barrier is reduced for carrier transport and the electronic density is rearranged in the system; thus, a nonlinear response is observed across the phase transition. In this way, the functional nonlinear electromagnetic composites are achieved by integrating metamaterials with phase-change materials, which can be tuned by a terahertz electric field in real time. Furthermore, a broadband electromagnetic response may be implemented in those composites by applying the aforementioned strategies for broadband functionalities. Recently, Abbaszadeh et al. reported that the mechanical strain can create a synthetic gauge field that controls the dynamics of electrons in the graphene sheets.[279] Upon tuning the strength of the gauge field, the density of states and the transverse spatial confinement of sound in the metamaterial can be effectively tuned. To some extent, active control with an external field provides a promising way to design the new generation of metamaterials that may dynamically modulate their physical properties, including the bandwidth, upon request.

Finally, we anticipate that the principles presented in this article, although initially coming from the electromagnetic systems, can be transferred to the related areas, such as acoustic metamaterials,[280,281] mechanical metamaterials,[279,282] and thermal metamaterials.[283,284] Material designing based on the basic physical principles is the first step to make devices with novel functionalities, which is the cornerstone of nowadays fast developing information technology. The concept of metamaterial, since it was first known to the world in 1999,[2] has brought us a large number of surprising and unexpected new physical properties. It is a good example of advanced materials with the artificially designed microstructures that their physical properties can be tailored to meet the exploding technology demands. On the road of exploring new metastructured materials with adaptive and sensitive broadband physical properties, we believe that the obstacles can surely be overcome with knowledge, imagination, and endeavors.

Acknowledgements

Conflict of Interest

The authors declare no conflict of interest.

ADVANCED
SCIENCE NEWS
www.advancedsciencenews.com

ADVANCED
MATERIALS
www.advmat.de

[1] T. W. Ebbesen, H. J. Lezec, H. F. Ghaemi, T. Thio, P. A. Wolff, *Nature* **1998**, *391*, 667.

[2] J. B. Pendry, A. J. Holden, D. J. Robbins, W. J. Stewart, *IEEE Trans. Microwave Theory Tech.* **1999**, *47*, 2075.

[3] J. B. Pendry, *Phys. Rev. Lett.* **2000**, *85*, 3966.

[4] R. A. Shelby, D. R. Smith, S. Schultz, *Science* **2001**, *292*, 77.

[5] D. R. Smith, J. B. Pendry, M. C. K. Wiltshire, *Science* **2004**, *305*, 788.

[6] Y. Liu, X. Zhang, *Chem. Soc. Rev.* **2011**, *40*, 2494.

[7] N. Yu, P. Genevet, M. A. Kats, F. Aieta, J.-P. Tetienne, F. Capasso, Z. Gaburro, *Science* **2011**, *334*, 333.

[8] A. V. Kildishev, A. Boltasseva, V. M. Shalaev, *Science* **2013**, *339*, 1232009.

[9] E. Hecht, *Optics*, 3rd ed., Addison-Wesley, Reading, MA **1997**.

[10] M. Born, E. Wolf, *Principles of Optics*, 7th ed., Cambridge University Press, Cambridge, UK **1999**.

[11] F. L. Pedrotti, L. M. Pedrotti, L. S. Pedrotti, *Introduction to Optics*, Cambridge University Press, Cambridge, UK **2017**.

[12] H. A. Atwater, A. Polman, *Nat. Mater.* **2010**, *9*, 205.

[13] F. Aieta, M. A. Kats, P. Genevet, F. Capasso, *Science* **2015**, *347*, 1342.

[14] P. Yu, L. V. Besteiro, Y. Huang, J. Wu, L. Fu, H. H. Tan, C. Jagadish, G. P. Wiederrecht, A. O. Govorov, Z. Wang, *Adv. Opt. Mater.* **2019**, *7*, 1800995.

[15] H.-T. Chen, J. Zhou, J. F. O'Hara, F. Chen, A. K. Azad, A. J. Taylor, *Phys. Rev. Lett.* **2010**, *105*, 073901.

[16] S.-C. Jiang, X. Xiong, Y.-S. Hu, Y.-H. Hu, G.-B. Ma, R.-W. Peng, C. Sun, M. Wang, *Phys. Rev. X* **2014**, *4*, 021026.

[17] N. K. Grady, J. E. Heyes, D. R. Chowdhury, Y. Zeng, M. T. Reiten, A. K. Azad, A. J. Taylor, D. A. R. Dalvit, H.-T. Chen, *Science* **2013**, *340*, 1304.

[18] S. Wang, P. C. Wu, V.-C. Su, Y.-C. Lai, C. H. Chu, J.-W. Chen, S.-H. Lu, J. Chen, B. Xu, C.-H. Kuan, T. Li, S. Zhu, D. P. Tsai, *Nat. Commun.* **2017**, *8*, 187.

[19] R. Liu, Q. Cheng, J. Y. Chin, J. J. Mock, T. J. Cui, D. R. Smith, *Opt. Express* **2009**, *17*, 21030.

[20] J. Zhu, G. V. Eleftheriades, *IEEE Antennas Wireless Propag. Lett.* **2009**, *8*, 295.

[21] M. Palandoken, A. Grede, H. Henke, *IEEE Trans. Antennas Propag.* **2009**, *57*, 331.

[22] N. R. Han, Z. C. Chen, C. S. Lim, B. Ng, M. H. Hong, *Opt. Express* **2011**, *19*, 6990.

[23] J. G. Ok, H. S. Youn, M. K. Kwak, K.-T. Lee, Y. J. Shin, L. J. Guo, A. Greenwald, Y. Liu, *Appl. Phys. Lett.* **2012**, *101*, 223102.

[24] C. Wang, Z. Y. Jia, K. Zhang, Y. Zhou, R. H. Fan, X. Xiong, R. W. Peng, *J. Appl. Phys.* **2014**, *115*, 244312.

[25] P. Moitra, B. A. Slovick, Z. G. Yu, S. Krishnamurthy, J. Valentine, *Appl. Phys. Lett.* **2014**, *104*, 171102.

[26] I. I. Smolyaninov, V. N. Smolyaninova, A. V. Kildishev, V. M. Shalaev, *Phys. Rev. Lett.* **2009**, *102*, 213901.

[27] R. Schittny, M. Kadic, T. Bückmann, M. Wegener, *Science* **2014**, *345*, 427.

[28] N. Wongkasem, A. Akyurtlu, J. Li, A. Tibolt, Z. Kang, W. D. Goodhue, *Prog. Electromagn. Res.* **2006**, *64*, 205.

[29] J. Valentine, S. Zhang, T. Zentgraf, E. Ulin-Avila, D. A. Genov, G. Bartal, X. Zhang, *Nature* **2008**, *455*, 376.

[30] K. L. Tsakmakidis, A. D. Boardman, O. Hess, *Nature* **2007**, *450*, 397.

[31] C. Wu, A. B. Khanikaev, G. Shvets, *Phys. Rev. Lett.* **2011**, *106*, 107403.

[32] H. Hu, D. Ji, X. Zeng, K. Liu, Q. Gan, *Sci. Rep.* **2013**, *3*, 1249.

[33] Z. Zhu, X. Yang, J. Gu, J. Jiang, W. Yue, Z. Tian, M. Tonouchi, J. Han, W. Zhang, *Nanotechnology* **2013**, *24*, 214003.

[34] Y. Xu, Y. Gu, B. Hou, Y. Lai, J. Li, H. Chen, *Nat. Commun.* **2013**, *4*, 2561.

[35] Z. Li, E. Palacios, S. Butun, K. Aydin, *Nano Lett.* **2015**, *15*, 1615.

[36] M. Choi, S. H. Lee, Y. Kim, S. B. Kang, J. Shin, M. H. Kwak, K.-Y. Kang, Y.-H. Lee, N. Park, B. Min, *Nature* **2011**, *470*, 369.

[37] Y. Yuan, C. Bingham, T. Tyler, S. Palit, T. H. Hand, W. J. Padilla, D. R. Smith, N. M. Jokerst, S. A. Cummer, *Opt. Express* **2008**, *16*, 9746.

[38] J. Wang, C. Fan, P. Ding, J. He, Y. Cheng, W. Hu, G. Cai, E. Liang, Q. Xue, *Opt. Express* **2012**, *20*, 14871.

[39] M. Pu, M. Wang, C. Hu, C. Huang, Z. Zhao, Y. Wang, X. Luo, *Opt. Express* **2012**, *20*, 25513.

[40] S. Bhattacharyya, S. Ghosh, K. V. Srivastava, *Microwave Opt. Technol. Lett.* **2013**, *55*, 2131.

[41] P. K. Singh, S. K. Ameri, L. Chao, M. N. Afsar, S. Sonkusale, *Prog. Electromagn. Res.* **2013**, *142*, 625.

[42] T. Cao, C.-W. Wei, R. E. Simpson, L. Zhang, M. J. Cryan, *Sci. Rep.* **2014**, *4*, 3955.

[43] C. Shi, X. Zang, Y. Wang, L. Chen, B. Cai, Y. Zhu, *Appl. Phys. Lett.* **2014**, *105*, 031104.

[44] W. Li, U. Guler, N. Kinsey, G. V. Naik, A. Boltasseva, J. Guan, V. M. Shalaev, A. V. Kildishev, *Adv. Mater.* **2014**, *26*, 7959.

[45] S. Ke, B. Wang, H. Huang, H. Long, K. Wang, P. Lu, *Opt. Express* **2015**, *23*, 8888.

[46] Y. Z. Cheng, W. Withayachumnankul, A. Upadhyay, D. Headland, Y. Nie, R. Z. Gong, M. Bhaskaran, S. Sriram, D. Abbott, *Adv. Opt Mater.* **2015**, *3*, 376.

[47] B. W. Du, W. Q. Yang, Q. Jiang, H. Y. Shan, D. Y. Luo, B. W. Li, W. C. Tang, F. Lin, B. Shen, Q. H. Gong, X. Zhu, R. Zhu, Z. Y. Fang, *Adv. Opt. Mater.* **2018**, *6*, 1701271.

[48] S. Chen, H. Cheng, H. Yang, J. Li, X. Duan, C. Gu, J. Tian, *Appl. Phys. Lett.* **2011**, *99*, 253104.

[49] C. Wu, G. Shvets, *Opt. Lett.* **2012**, *37*, 308.

[50] Y. Gu, L. J. Wang, P. Ren, J. X. Zhang, T. C. Zhang, O. J. F. Martin, Q. H. Gong, *Nano Lett.* **2012**, *12*, 2488.

[51] Y. Peng, X. Zang, Y. Zhu, C. Shi, L. Chen, B. Cai, S. Zhuang, *Opt. Express* **2015**, *23*, 2032.

[52] X. Zang, C. Shi, L. Chen, B. Cai, Y. Zhu, S. Zhuang, *Sci. Rep.* **2015**, *5*, 8901.

[53] N. Zhang, P. Zhou, S. Wang, X. Weng, J. Xie, L. Deng, *Opt. Commun.* **2015**, *338*, 388.

[54] J. Yoon, M. Zhou, M. A. Badsha, T. Y. Kim, Y. C. Jun, C. K. Hwangbo, *Sci. Rep.* **2015**, *5*, 12788.

[55] S. Bhattacharyya, S. Ghosh, D. Chaurasiya, K. V. Srivastava, *IET Microw. Antennas Propag.* **2015**, *9*, 1160.

[56] D. Hu, J. Cao, W. Li, C. Zhang, T. Wu, Q. Li, Z. Chen, Y. Wang, J. Guan, *Adv. Opt. Mater.* **2017**, *5*, 1700109.

[57] Y. Huang, J. Luo, M. Pu, Y. Guo, Z. Zhao, X. Ma, X. Li, X. Luo, *Adv. Sci.* **2019**, *6*, 1801691.

[58] H. Wakatsuchi, S. Greedy, C. Christopoulos, J. Paul, *Opt. Express* **2010**, *18*, 22187.

[59] J. Grant, Y. Ma, S. Saha, A. Khalid, D. R. S. Cumming, *Opt. Lett.* **2011**, *36*, 3476.

[60] Y. Cheng, Y. Nie, R. Gong, *Appl. Phys. B* **2013**, *111*, 483.

[61] S. Bhattacharyya, S. Ghosh, K. V. Srivastava, *J. Appl. Phys.* **2013**, *114*, 094514.

1904646 (18 of 22)

**ADVANCED
SCIENCE NEWS**

www.advancedsciencenews.com

**ADVANCED
MATERIALS**

www.advmat.de

[62] W. Ma, Y. Wen, X. Yu, *Opt. Express* **2013**, *21*, 30724.

[63] B.-X. Wang, L.-L. Wang, G.-Z. Wang, W.-Q. Huang, X.-F. Li, X. Zhai, *IEEE Photonics Technol. Lett.* **2014**, *26*, 111.

[64] B.-Y. Wang, S.-B. Liu, B.-R. Bian, Z.-W. Mao, X.-C. Liu, B. Ma, L. Chen, *J. Appl. Phys.* **2014**, *116*, 094504.

[65] X. Duan, S. Chen, W. Liu, H. Cheng, Z. Li, J. Tian, *J. Opt.* **2014**, *16*, 125107.

[66] X.-J. He, S.-T. Yan, Q.-X. Ma, Q.-F. Zhang, P. Jia, F.-M. Wu, J.-X. Jiang, *Opt. Commun.* **2015**, *340*, 44.

[67] C. Gong, M. Zhan, J. Yang, Z. Wang, H. Liu, Y. Zhao, W. Liu, *Sci. Rep.* **2016**, *6*, 32466.

[68] J. Dai, C. X. Xu, R. Ding, K. Zheng, Z. L. Shi, C. G. Lv, Y. P. Cui, *Appl. Phys. Lett.* **2009**, *95*, 191117.

[69] R.-M. Ma, R. F. Oulton, V. J. Sorger, G. Bartal, X. Zhang, *Nat. Mater.* **2011**, *10*, 110.

[70] D. R. Chowdhury, R. Singh, M. Reiten, H.-T. Chen, A. J. Taylor, J. F. O'Hara, A. K. Azad, *Opt. Express* **2011**, *19*, 15817.

[71] Y. Yao, J. Yao, V. K. Narasimhan, Z. Ruan, C. Xie, S. Fan, Y. Cui, *Nat. Commun.* **2012**, *3*, 664.

[72] Y. Liu, S. Gu, C. Luo, X. Zhao, *Appl. Phys. A* **2012**, *108*, 19.

[73] D. Wen, H. Yang, Q. Ye, M. Li, L. Guo, J. Zhang, *Phys. Scr.* **2013**, *88*, 015402.

[74] X. Chen, H. Gong, S. Dai, D. Zhao, Y. Yang, Q. Li, M. Qiu, *Opt. Lett.* **2013**, *38*, 2247.

[75] H. Xiong, J.-S. Hong, C.-M. Luo, L.-L. Zhong, *J. Appl. Phys.* **2013**, *114*, 064109.

[76] M. Amin, M. Farhat, H. Bağcı, *Opt. Express* **2013**, *21*, 29938.

[77] L. Meng, D. Zhao, Q. Li, M. Qiu, *Opt. Express* **2013**, *21*, A111.

[78] W. Li, T. Wu, W. Wang, J. Guan, P. Zhai, *Appl. Phys. Lett.* **2014**, *104*, 022903.

[79] J. A. Bossard, L. Lin, S. Yun, L. Liu, D. H. Werner, T. S. Mayer, *ACS Nano* **2014**, *8*, 1517.

[80] T. Jang, H. Youn, Y. J. Shin, L. J. Guo, *ACS Photonics* **2014**, *1*, 279.

[81] D. T. Viet, N. T. Hien, P. V. Tuong, N. Q. Minh, P. T. Trang, L. N. Le, Y. P. Lee, V. D. Lam, *Opt. Commun.* **2014**, *322*, 209.

[82] G.-H. Yang, X.-X. Liu, Y.-L. Lv, J.-H. Fu, Q. Wu, X. Gu, *J. Appl. Phys.* **2014**, *115*, 17E523.

[83] Y. Guo, L. Yan, W. Pan, B. Luo, X. Luo, *Plasmonics* **2014**, *9*, 951.

[84] R. Ning, S. Liu, H. Zhang, X. Kong, B. Bian, J. Bao, *J. Opt.* **2014**, *16*, 125108.

[85] S. Li, J. Gao, X. Cao, Z. Zhang, Y. Zheng, C. Zhang, *Opt. Express* **2015**, *23*, 3523.

[86] S. Liu, H. Chen, T. J. Cui, *Appl. Phys. Lett.* **2015**, *106*, 151601.

[87] W. Guo, Y. Liu, T. Han, *Opt. Express* **2016**, *24*, 20586.

[88] H. Wei, F. Hao, Y. Z. Huang, W. Z. Wang, P. Nordlander, H. X. Xu, *Nano Lett.* **2008**, *8*, 2497.

[89] J. F. Li, Y. F. Huang, Y. Ding, Z. L. Yang, S. B. Li, X. S. Zhou, F. R. Fan, W. Zhang, Z. Y. Zhou, D. Y. Wu, B. Ren, Z. L. Wang, Z. Q. Tian, *Nature* **2010**, *464*, 392.

[90] K. Aydin, V. E. Ferry, R. M. Briggs, H. A. Atwater, *Nat. Commun.* **2011**, *2*, 517.

[91] S. Butun, K. Aydin, *Opt. Express* **2014**, *22*, 19457.

[92] F. Ding, Y. Cui, X. Ge, Y. Jin, S. He, *Appl. Phys. Lett.* **2012**, *100*, 103506.

[93] D. Ji, H. Song, X. Zeng, H. Hu, K. Liu, N. Zhang, Q. Gan, *Sci. Rep.* **2014**, *4*, 4498.

[94] S. He, F. Ding, L. Mo, F. Bao, *Prog. Electromagn. Res.* **2014**, *147*, 69.

[95] J. Zhou, A. F. Kaplan, L. Chen, L. J. Guo, *ACS Photonics* **2014**, *1*, 618.

[96] J. Zhu, Z. Ma, W. Sun, F. Ding, Q. He, L. Zhou, Y. Ma, *Appl. Phys. Lett.* **2014**, *105*, 021102.

[97] F. Ding, Y. Jin, B. Li, H. Cheng, L. Mo, S. He, *Laser Photonics Rev.* **2014**, *8*, 946.

[98] Y. J. Kim, Y. J. Yoo, K. W. Kim, J. Y. Rhee, Y. H. Kim, Y. P. Lee, *Opt. Express* **2015**, *23*, 3861.

[99] X. Yin, C. Long, J. Li, H. Zhu, L. Chen, J. Guan, X. Li, *Sci. Rep.* **2015**, *5*, 15367.

[100] Y. Pang, J. Wang, H. Ma, M. Feng, Y. Li, Z. Xu, S. Xia, S. Qu, *Sci. Rep.* **2016**, *6*, 29429.

[101] M. M. Hossain, B. Jia, M. Gu, *Adv. Opt. Mater.* **2015**, *3*, 1047.

[102] R. Zhang, Y. Zhang, Z. C. Dong, S. Jiang, C. Zhang, L. G. Chen, L. Zhang, Y. Liao, J. Aizpurua, Y. Luo, J. L. Yang, J. G. Hou, *Nature* **2013**, *498*, 82.

[103] B. B. Mandelbrot, *The Fractal Geometry of Nature* Freeman, New York **1983**.

[104] Y.-J. Bao, B. Zhang, Z. Wu, J.-W. Si, M. Wang, R.-W. Peng, X. Lu, J. Shao, Z.-F. Li, X.-P. Hao, N.-B. Ming, *Appl. Phys. Lett.* **2007**, *90*, 251914.

[105] G. Volpe, G. Volpe, R. Quidant, *Opt. Express* **2011**, *19*, 3612.

[106] L.-H. Zhu, M.-R. Shao, R.-W. Peng, R.-H. Fan, X.-R. Huang, M. Wang, *Opt. Express* **2013**, *21*, A313.

[107] B. Q. Chen, C. Zhang, C. Y. Hu, R. J. Liu, Z. Y. Li, *Phys. Rev. Lett.* **2015**, *115*, 083902.

[108] S. Gottheim, H. Zhang, A. O. Govorov, N. J. Halas, *ACS Nano* **2015**, *9*, 3284.

[109] R. S. Hegde, E. H. Khoo, *Plasmonics* **2016**, *11*, 465.

[110] E. Aslan, E. Aslan, R. Wang, M. K. Hong, S. Erramilli, M. Turkmen, O. G. Saracoglu, L. D. Negro, *ACS Photonics* **2016**, *3*, 2102.

[111] A. E. Dorche, S. Abdollahramezani, A. Chizari, A. Khavasi, *IEEE Photonics Technol. Lett.* **2016**, *28*, 2545.

[112] Y. Wen, S. Liu, H. Zhang, L. Wang, *Plasmonics* **2018**, *13*, 1767.

[113] N. Fernez, Y. Arbaoui, A. Maalouf, A. Chevalier, P. Agaciak, L. Burgnies, P. Queffelec, V. Laur, É. Lheurette, *J. Appl. Phys.* **2018**, *123*, 084902.

[114] F. De Nicola, N. S. P. Purayil, D. Spirito, M. Miscuglio, F. Tantussi, A. Tomadin, F. De Angelis, M. Polini, R. Krahne, V. Pellegrini, *ACS Photonics* **2018**, *5*, 2418.

[115] G. Q. Wallace, F. Lagugné-Labarthet, *Analyst* **2019**, *144*, 13.

[116] M. K. Hedayati, F. Faupel, M. Elbahri, *Appl. Phys. A* **2012**, *109*, 769.

[117] Y. Zhang, B. Dong, A. Chen, X. Liu, L. Shi, J. Zi, *Adv. Mater.* **2015**, *27*, 4719.

[118] Z. Liu, X. Liu, S. Huang, P. Pan, J. Chen, G. Liu, G. Gu, *ACS Appl. Mater. Interfaces* **2015**, *7*, 4962.

[119] L. Zhou, Y. Tan, D. Ji, B. Zhu, P. Zhang, J. Xu, Q. Gan, Z. Yu, J. Zhu, *Sci. Adv.* **2016**, *2*, e1501227.

[120] S. Sun, K.-Y. Yang, C.-M. Wang, T.-K. Juan, W. T. Chen, C. Y. Liao, Q. He, S. Xiao, W.-T. Kung, G.-Y. Guo, L. Zhou, D. P. Tsai, *Nano Lett.* **2012**, *12*, 6223.

[121] A. Pors, M. G. Nielsen, R. L. Eriksen, S. I. Bozhevolnyi, *Nano Lett.* **2013**, *13*, 829.

[122] A. Pors, S. I. Bozhevolnyi, *Opt. Express* **2013**, *21*, 2942.

[123] H. Cheng, S. Chen, P. Yu, J. Li, B. Xie, Z. Li, J. Tian, *Appl. Phys. Lett.* **2013**, *103*, 223102.

[124] Q. Lévesque, M. Makhsiyan, P. Bouchon, F. Pardo, J. Jaeck, N. Bardou, C. Dupuis, R. Haïdar, J.-L. Pelouard, *Appl. Phys. Lett.* **2014**, *104*, 111105.

[125] F. Ding, Z. Wang, S. He, V. M. Shalaev, A. V. Kildishev, *ACS Nano* **2015**, *9*, 4111.

[126] D. Wen, F. Yue, G. Li, G. Zheng, K. Chan, S. Chen, M. Chen, K. F. Li, P. W. H. Wong, K. W. Cheah, E. Y. B. Pun, S. Zhang, X. Chen, *Nat. Commun.* **2015**, *6*, 8241.

[127] Y. Guo, L. Yan, W. Pan, B. Luo, *Opt. Express* **2015**, *23*, 27566.

[128] S.-C. Jiang, X. Xiong, Y.-S. Hu, S.-W. Jiang, Y.-H. Hu, D.-H. Xu, R.-W. Peng, M. Wang, *Phys. Rev. B* **2015**, *91*, 125421.

[129] H. Shi, J. Li, A. Zhang, J. Wang, Z. Xu, *Opt. Express* **2014**, *22*, 20973.

[130] N. Yu, F. Capasso, *Nat. Mater.* **2014**, *13*, 139.

[131] P. Genevet, F. Capasso, F. Aieta, M. Khorasaninejad, R. Devlin, *Optica* **2017**, *4*, 139.

1904646 (19 of 22)

**ADVANCED
SCIENCE NEWS**

www.advancedsciencenews.com

**ADVANCED
MATERIALS**

www.advmat.de

[132] G. Zheng, H. Mühlenbernd, M. Kenney, G. Li, T. Zentgraf, S. Zhang, *Nat. Nanotechnol.* **2015**, *10*, 308.

[133] M. Khorasaninejad, F. Capasso, *Science* **2017**, *358*, eaam8100.

[134] J. Zhong, N. An, N. Yi, M. Zhu, Q. Song, S. Xiao, *Plasmonics* **2016**, *11*, 537.

[135] Z. Wei, Y. Cao, Y. Fan, X. Yu, H. Li, *Appl. Phys. Lett.* **2011**, *99*, 221907.

[136] Y. Z. Cheng, Y. Nie, Z. Z. Cheng, L. Wu, X. Wang, R. Z. Gong, *J. Electromagn. Waves Appl.* **2013**, *27*, 1850.

[137] M. Feng, J. Wang, H. Ma, W. Mo, H. Ye, S. Qu, *J. Appl. Phys.* **2013**, *114*, 074508.

[138] L. Cong, W. Cao, X. Zhang, Z. Tian, J. Gu, R. Singh, J. Han, W. Zhang, *Appl. Phys. Lett.* **2013**, *103*, 171107.

[139] H. S. Park, T.-T. Kim, H.-D. Kim, K. Kim, B. Min, *Nat. Commun.* **2014**, *5*, 5435.

[140] R.-H. Fan, Y. Zhou, X.-P. Ren, R.-W. Peng, S.-C. Jiang, D.-H. Xu, X. Xiong, X.-R. Huang, M. Wang, *Adv. Mater.* **2015**, *27*, 1201.

[141] C. P. Huang, Q. J. Wang, X. G. Yin, Y. Zhang, J. Q. Li, Y. Y. Zhu, *Adv. Opt. Mater.* **2014**, *2*, 723.

[142] L. Huang, X. Chen, H. Müehlenbernd, G. Li, B. Bai, Q. Tan, G. Jin, T. Zentgraf, S. Zhang, *Nano Lett.* **2012**, *12*, 5750.

[143] L. Cong, N. Xu, J. Han, W. Zhang, R. Singh, *Adv. Mater.* **2015**, *27*, 6630.

[144] S. Choudhury, U. Guler, A. Shaltout, V. M. Shalaev, A. V. Kildishev, A. Boltasseva, *Adv. Opt. Mater.* **2017**, *5*, 1700196.

[145] D. Lin, P. Fan, E. Hasman, M. L. Brongersma, *Science* **2014**, *345*, 298.

[146] K. Huang, Z. Dong, S. Mei, L. Zhang, Y. Liu, H. Liu, H. Zhu, J. Teng, B. Luk'yanchuk, J. K. W. Yang, C.-W. Qiu, *Laser Photonics Rev.* **2016**, *10*, 500.

[147] Y.-W. Huang, W. T. Chen, W.-Y. Tsai, P. C. Wu, C.-M. Wang, G. Sun, D. P. Tsai, *Nano Lett.* **2015**, *15*, 3122.

[148] O. Avayu, E. Almeida, Y. Prior, T. Ellenbogen, *Nat. Commun.* **2017**, *8*, 14992.

[149] M. Khorasaninejad, Z. Shi, A. Y. Zhu, W. T. Chen, V. Sanjeev, A. Zaidi, F. Capasso, *Nano Lett.* **2017**, *17*, 1819.

[150] S. Wang, P. C. Wu, V.-C. Su, Y.-C. Lai, M.-K. Chen, H. Y. Kuo, B. H. Chen, Y. H. Chen, T.-T. Huang, J.-H. Wang, R.-M. Lin, C.-H. Kuan, T. Li, Z. Wang, S. Zhu, D. P. Tsai, *Nat. Nanotechnol.* **2018**, *13*, 227.

[151] W. T. Chen, A. Y. Zhu, V. Sanjeev, M. Khorasaninejad, Z. Shi, E. Lee, F. Capasso, *Nat. Nanotechnol.* **2018**, *13*, 220.

[152] C. Wu, H. Li, X. Yu, F. Li, H. Chen, C. T. Chan, *Phys. Rev. Lett.* **2011**, *107*, 177401.

[153] J. K. Gansel, M. Thiel, M. S. Rill, M. Decker, K. Bade, V. Saile, G. von Freymann, S. Linden, M. Wegener, *Science* **2009**, *325*, 1513.

[154] C. Wu, H. Li, Z. Wei, X. Yu, C. T. Chan, *Phys. Rev. Lett.* **2010**, *105*, 247401.

[155] Z. Y. Yang, M. Zhao, P. X. Lu, Y. F. Lu, *Opt. Lett.* **2010**, *35*, 2588.

[156] Y. Zhao, M. A. Belkin, A. Alù, *Nat. Commun.* **2012**, *3*, 870.

[157] J. Kaschke, J. K. Gansel, M. Wegener, *Opt. Express* **2012**, *20*, 26012.

[158] J. Kaschke, L. Blume, L. Wu, M. Thiel, K. Bade, Z. Yang, M. Wegener, *Adv. Opt. Mater.* **2015**, *3*, 1411.

[159] R. Ji, S.-W. Wang, X. Liu, X. Chen, W. Lu, *Nanoscale* **2016**, *8*, 14725.

[160] M. A. Kats, P. Genevet, G. Aoust, N. Yu, R. Blanchard, F. Aieta, Z. Gaburro, F. Capasso, *Proc. Natl. Acad. Sci. USA* **2012**, *109*, 12364.

[161] N. Yu, F. Aieta, P. Genevet, M. A. Kats, Z. Gaburro, F. Capasso, *Nano Lett.* **2012**, *12*, 6328.

[162] X. Ni, N. K. Emani, A. V. Kildishev, A. Boltasseva, V. M. Shalaev, *Science* **2012**, *335*, 427.

[163] Y. Zhao, A. Alù, *Nano Lett.* **2013**, *13*, 1086.

[164] X. Xiong, Y.-S. Hu, S.-C. Jiang, Y.-H. Hu, R.-H. Fan, G.-B. Ma, D.-J. Shu, R.-W. Peng, M. Wang, *Appl. Phys. Lett.* **2014**, *105*, 201105.

[165] Z. Li, S. Chen, W. Liu, H. Cheng, Z. Liu, J. Li, P. Yu, B. Xie, J. Tian, *Plasmonics* **2015**, *10*, 1703.

[166] W. Liu, S. Chen, Z. Li, H. Cheng, P. Yu, J. Li, J. Tian, *Opt. Lett.* **2015**, *40*, 3185.

[167] L. Chen, X. Ke, H. Guo, J. Li, X. Li, L. Zhou, *Sci. Rep.* **2018**, *8*, 1051.

[168] J. Li, J. B. Pendry, *Phys. Rev. Lett.* **2008**, *101*, 203901.

[169] E. Kallos, C. Argyropoulos, Y. Hao, *Phys. Rev. A* **2009**, *79*, 063825.

[170] J. Renger, M. Kadic, G. Dupont, S. S. Aćimović, S. Guenneau, R. Quidant, S. Enoch, *Opt. Express* **2010**, *18*, 15757.

[171] D. Shin, Y. Urzhumov, Y. Jung, G. Kang, S. Baek, M. Choi, H. Park, K. Kim, D. R. Smith, *Nat. Commun.* **2012**, *3*, 1213.

[172] H. F. Ma, T. J. Cui, *Nat. Commun.* **2010**, *1*, 124.

[173] C. Sheng, H. Liu, Y. Wang, S. N. Zhu, D. A. Genov, *Nat. Photonics* **2013**, *7*, 902.

[174] L. Wu, X. Tian, H. Ma, M. Yin, D. Li, *Appl. Phys. Lett.* **2013**, *102*, 074103.

[175] M. Yin, X. Y. Tian, L. L. Wu, D. C. Li, *Appl. Phys. Lett.* **2014**, *104*, 094101.

[176] D. Jia, Y. He, N. Ding, J. Zhou, B. Du, W. Zhang, *IEEE Antennas Wireless Propag. Lett.* **2018**, *17*, 1510.

[177] B. Vasić, G. Isić, R. Gajić, K. Hingerl, *Opt. Express* **2010**, *18*, 20321.

[178] Y. Shen, D. Ye, I. Celanovic, S. G. Johnson, J. D. Joannopoulos, M. Soljačić, *Science* **2014**, *343*, 1499.

[179] P. H. Q. Pham, W. Zhang, N. V. Quach, J. Li, W. Zhou, D. Scarmardo, E. R. Brown, P. J. Burke, *Nat. Commun.* **2017**, *8*, 2233.

[180] M. Liu, X. Yin, E. Ulin-Avila, B. Geng, T. Zentgraf, L. Ju, F. Wang, X. Zhang, *Nature* **2011**, *474*, 64.

[181] L. Ren, Q. Zhang, J. Yao, Z. Sun, R. Kaneko, Z. Yan, S. Nanot, Z. Jin, I. Kawayama, M. Tonouchi, J. M. Tour, J. Kono, *Nano Lett.* **2012**, *12*, 3711.

[182] W. Li, B. Chen, C. Meng, W. Fang, Y. Xiao, X. Li, Z. Hu, Y. Xu, L. Tong, H. Wang, W. Liu, J. Bao, Y. R. Shen, *Nano Lett.* **2014**, *14*, 955.

[183] Z. Qiao, W. Ren, H. Chen, L. Bellaiche, Z. Zhang, A. H. MacDonald, Q. Niu, *Phys. Rev. Lett.* **2014**, *112*, 116404.

[184] Q. Li, Z. Tian, X. Zhang, R. Singh, L. Du, J. Gu, J. Han, W. Zhang, *Nat. Commun.* **2015**, *6*, 7082.

[185] X. Liu, Z. Chen, E. P. J. Parrott, B. S.-Y. Ung, J. Xu, E. Pickwell-MacPherson, *Adv. Opt. Mater.* **2017**, *5*, 1600697.

[186] Z. Huang, H. Chen, Y. Huang, Z. Ge, Y. Zhou, Y. Yang, P. Xiao, J. Liang, T. Zhang, Q. Shi, G. Li, Y. Chen, *Adv. Funct. Mater.* **2018**, *28*, 1704363.

[187] Z. Chen, X. Chen, L. Tao, K. Chen, M. Long, X. Liu, K. Yan, R. I. Stantchev, E. Pickwell-MacPherson, J.-B. Xu, *Nat. Commun.* **2018**, *9*, 4909.

[188] H. Lin, B. C. P. Sturmberg, K.-T. Lin, Y. Yang, X. Zheng, T. K. Chong, C. M. de Sterke, B. Jia, *Nat. Photonics* **2019**, *13*, 270.

[189] R. Liu, C. Ji, J. J. Mock, J. Y. Chin, T. J. Cui, D. R. Smith, *Science* **2009**, *323*, 366.

[190] J. Valentine, J. Li, T. Zentgraf, G. Bartal, X. Zhang, *Nat. Mater.* **2009**, *8*, 568.

[191] S. Tretyakov, P. Alitalo, O. Luukkonen, C. Simovski, *Phys. Rev. Lett.* **2009**, *103*, 103905.

[192] H. F. Ma, W. X. Jiang, X. M. Yang, X. Y. Zhou, T. J. Cui, *Opt. Express* **2009**, *17*, 19947.

[193] X. Liu, C. Li, K. Yao, X. Meng, F. Li, *IEEE Antennas Wireless Propag. Lett.* **2009**, *8*, 1154.

[194] C. Li, X. Liu, F. Li, *Phys. Rev. B* **2010**, *81*, 115133.

[195] C. Li, X. Meng, X. Liu, F. Li, G. Fang, H. Chen, C. T. Chan, *Phys. Rev. Lett.* **2010**, *105*, 233906.

[196] M. Gharghi, C. Gladden, T. Zentgraf, Y. Liu, X. Yin, J. Valentine, X. Zhang, *Nano Lett.* **2011**, *11*, 2825.

[197] T. Nagayama, A. Sanada, *IEEE Trans. Microwave Theory Tech.* **2015**, *63*, 3851.

1904646 (20 of 22)

[198] Y. Deng, S. Xu, R. Zhang, B. Zheng, H. Chen, F. Gao, F. Yu, B. Zhang, H. Chen, *J. Opt.* **2016**, *18*, 044006.

[199] S. Khosravi, A. Rostami, M. Dolatyari, G. Rostami, *IEEE Trans. Nanotechnol.* **2017**, *16*, 44.

[200] J. Neu, B. Krolla, O. Paul, B. Reinhard, R. Beigang, M. Rahm, *Opt. Express* **2010**, *18*, 27748.

[201] N. Kundtz, D. R. Smith, *Nat. Mater.* **2010**, *9*, 129.

[202] Z. H. Jiang, M. D. Gregory, D. H. Werner, *IEEE Trans. Antennas Propag.* **2012**, *60*, 5063.

[203] A. Dhouibi, S. N. Burokur, A. de Lustrac, A. Priou, *Appl. Phys. Lett.* **2013**, *102*, 024102.

[204] B. Zheng, R. Zhang, M. Zhou, W. Zhang, S. Lin, Z. Ni, H. Wang, F. Yu, H. Chen, *Appl. Phys. Lett.* **2014**, *104*, 073502.

[205] H.-X. Xu, G.-M. Wang, Z. Tao, T. J. Cui, *Sci. Rep.* **2014**, *4*, 5744.

[206] M. Q. Qi, W. X. Tang, T. J. Cui, *Sci. Rep.* **2015**, *5*, 11732.

[207] H. F. Ma, X. Chen, X. M. Yang, H. S. Xu, Q. Cheng, T. J. Cui, *Chin. Sci. Bull.* **2010**, *55*, 2066.

[208] X. Chen, H. F. Ma, X. Y. Zou, W. X. Jiang, T. J. Cui, *J. Appl. Phys.* **2011**, *110*, 044904.

[209] Z. L. Mei, J. Bai, T. M. Niu, T. J. Cui, *IEEE Trans. Antennas Propag.* **2012**, *60*, 398.

[210] A. Dhouibi, S. N. Burokur, A. de Lustrac, A. Priou, *IEEE Antennas Wireless Propag. Lett.* **2012**, *11*, 1504.

[211] A. Dhouibi, S. N. Burokur, A. de Lustrac, A. Priou, *IEEE Antennas Wireless Propag. Lett.* **2013**, *12*, 43.

[212] Q. Wu, Z. H. Jiang, O. Quevedo-Teruel, J. P. Turpin, W. Tang, Y. Hao, D. H. Werner, *IEEE Trans. Antennas Propag.* **2013**, *61*, 5910.

[213] G. Yuan, X. Dong, Q. Deng, C. Liu, Y. Lu, H. Shi, C. Du, *Microwave Opt. Technol. Lett.* **2014**, *56*, 1124.

[214] A. Dhouibi, S. N. Burokur, A. de Lustrac, *J. Appl. Phys.* **2014**, *115*, 194901.

[215] L. Chen, Z. Lei, R. Yang, J. Fan, X. Shi, *IEEE Trans. Antennas Propag.* **2015**, *63*, 395.

[216] S. Genovesi, F. Costa, F. Fanciulli, A. Monorchio, *IEEE Antennas Wireless Propag. Lett.* **2016**, *15*, 1927.

[217] E. Erfani, M. Niroo-Jazi, S. Tatu, *IEEE Trans. Antennas Propag.* **2016**, *64*, 1968.

[218] W. Lee, Y. J. Yoon, *IEEE Antennas Wireless Propag. Lett.* **2017**, *16*, 856.

[219] Q.-W. Lin, H. Wong, *IEEE Trans. Antennas Propag.* **2018**, *66*, 5764.

[220] R. Singha, D. Vakula, *Int. J. RF Microwave Comput. Aided Eng.* **2018**, *28*, e21191.

[221] N. I. Landy, W. J. Padilla, *Opt. Express* **2009**, *17*, 14872.

[222] D. Liu, Z. Xu, N. Ma, S. Zhang, *Appl. Phys. A* **2012**, *106*, 949.

[223] M. Lapine, A. K. Krylova, P. A. Belov, C. G. Poulton, R. C. McPhedran, Y. S. Kivshar, *Phys. Rev. B* **2013**, *87*, 024408.

[224] K. Chung, R. Kim, T. Chang, J. Shin, *Appl. Phys. Lett.* **2016**, *109*, 021114.

[225] D. R. Smith, D. Schurig, *Phys. Rev. Lett.* **2003**, *90*, 077405.

[226] A. Poddubny, I. Iorsh, P. Belov, Y. Kivshar, *Nat. Photonics* **2013**, *7*, 958.

[227] P. Huo, S. Zhang, Y. Liang, Y. Lu, T. Xu, *Adv. Opt. Mater.* **2019**, *7*, 1801616.

[228] Y. Liu, G. Bartal, X. Zhang, *Opt. Express* **2008**, *16*, 15439.

[229] J. Yao, Z. Liu, Y. Liu, Y. Wang, C. Sun, G. Bartal, A. M. Stacy, X. Zhang, *Science* **2008**, *321*, 930.

[230] Z. Jacob, L. V. Alekseyev, E. Narimanov, *Opt. Express* **2006**, *14*, 8247.

[231] Z. Liu, H. Lee, Y. Xiong, C. Sun, X. Zhang, *Science* **2007**, *315*, 1686.

[232] A. J. Hoffman, L. Alekseyev, S. S. Howard, K. J. Franz, D. Wasserman, V. A. Podolskiy, E. E. Narimanov, D. L. Sivco, C. Gmachl, *Nat. Mater.* **2007**, *6*, 946.

[233] C. T. Riley, J. S. T. Smalley, J. R. J. Brodie, Y. Fainman, D. J. Sirbuly, Z. Liu, *Proc. Natl. Acad. Sci. USA* **2017**, *114*, 1264.

[234] J. B. Pendry, L. Martín-Moreno, F. J. Garcia-Vidal, *Science* **2004**, *305*, 847.

[235] X.-R. Huang, R.-W. Peng, R.-H. Fan, *Phys. Rev. Lett.* **2010**, *105*, 243901.

[236] R.-H. Fan, R.-W. Peng, X.-R. Huang, J. Li, Y. Liu, Q. Hu, M. Wang, X. Zhang, *Adv. Mater.* **2012**, *24*, 1980.

[237] N. Aköezbek, N. Mattiucci, D. de Ceglia, R. Trimm, A. Alù, G. D'Aguanno, M. A. Vincenti, M. Scalora, M. J. Bloemer, *Phys. Rev. B* **2012**, *85*, 205430.

[238] R.-H. Fan, L.-H. Zhu, R.-W. Peng, X.-R. Huang, D.-X. Qi, X.-P. Ren, Q. Hu, M. Wang, *Phys. Rev. B* **2013**, *87*, 195444.

[239] A. Alù, G. D'Aguanno, N. Mattiucci, M. J. Bloemer, *Phys. Rev. Lett.* **2011**, *106*, 123902.

[240] R.-H. Fan, J. Li, R.-W. Peng, X.-R. Huang, D.-X. Qi, D.-H. Xu, X.-P. Ren, M. Wang, *Appl. Phys. Lett.* **2013**, *102*, 171904.

[241] X.-P. Ren, R.-H. Fan, R.-W. Peng, X.-R. Huang, D.-H. Xu, Y. Zhou, M. Wang, *Phys. Rev. B* **2015**, *91*, 045111.

[242] C. Argyropoulos, G. D'Aguanno, N. Mattiucci, N. Akozbek, M. J. Bloemer, A. Alù, *Phys. Rev. B* **2012**, *85*, 024304.

[243] H. Shen, B. Maes, *Appl. Phys. Lett.* **2012**, *100*, 241104.

[244] A. Maurel, S. Félix, J.-F. Mercier, *Phys. Rev. B* **2013**, *88*, 115416.

[245] N. Mattiucci, M. J. Bloemer, N. Aközbek, G. D'Aguanno, *Sci. Rep.* **2013**, *3*, 3203.

[246] M. J. Bloemer, N. Mattiucci, G. D'Aguanno, R. Trimm, N. Akozbek, *Appl. Phys. Lett.* **2014**, *104*, 021103.

[247] K. Q. Le, *J. Appl. Phys.* **2014**, *115*, 033110.

[248] W. Zhang, Y. Wang, L. Luo, G. Li, Z. Zhang, *Plasmonics* **2015**, *10*, 547.

[249] T. Søndergaard, S. M. Novikov, T. Holmgaard, R. L. Eriksen, J. Beermann, Z. Han, K. Pedersen, S. I. Bozhevolnyi, *Nat. Commun.* **2012**, *3*, 969.

[250] K. Q. Le, C. Argyropoulos, N. Mattiucci, G. D'Aguanno, M. J. Bloemer, A. Alù, *J. Appl. Phys.* **2012**, *112*, 094317.

[251] C. Argyropoulos, K. Q. Le, N. Mattiucci, G. D'Aguanno, A. Alù, *Phys. Rev. B* **2013**, *87*, 205112.

[252] Y.-K. Wang, Y. Qin, Z.-Y. Zhang, *IEEE Photonics J.* **2014**, *6*, 4801508.

[253] D. X. Qi, R. H. Fan, R. W. Peng, X. R. Huang, M. H. Lu, X. Ni, Q. Hu, M. Wang, *Appl. Phys. Lett.* **2012**, *101*, 061912.

[254] D. X. Qi, Y. Q. Deng, D. H. Xu, R. H. Fan, R. W. Peng, Z. G. Chen, M. H. Lu, X. R. Huang, M. Wang, *Appl. Phys. Lett.* **2015**, *106*, 011906.

[255] G. Subramania, S. Foteinopoulou, I. Brener, *Phys. Rev. Lett.* **2011**, *107*, 163902.

[256] A. Novitsky, A. M. Ivinskaya, M. Zalkovskij, R. Malureanu, P. U. Jepsen, A. V. Lavrinenko, *J. Appl. Phys.* **2012**, *112*, 074318.

[257] A. Pors, K. V. Nerkararyan, K. Sahakyan, S. I. Bozhevolnyi, *Opt. Lett.* **2016**, *41*, 242.

[258] Y. A. Akimov, W. S. Koh, *Plasmonics* **2011**, *6*, 155.

[259] H. C. Hwang, K. Park, W.-K. Park, S.-T. Han, K. R. Kim, *Jpn. J. Appl. Phys.* **2012**, *51*, 06FE17.

[260] O. V. Polischuk, V. V. Popov, W. Knap, *Semiconductors* **2015**, *49*, 104.

[261] H. Ren, X. Li, Q. Zhang, M. Gu, *Science* **2016**, *352*, 805.

[262] S. Gu, J. P. Barrett, T. H. Hand, B.-I. Popa, S. A. Cummer, *J. Appl. Phys.* **2010**, *108*, 064913.

[263] Y. Z. Cheng, Y. Wang, Y. Nie, R. Z. Gong, X. Xiong, X. Wang, *J. Appl. Phys.* **2012**, *111*, 044902.

[264] J. Chen, X. Huang, G. Zerihun, Z. Hu, S. Wang, G. Wang, X. Hu, M. Liu, *J. Electron. Mater.* **2015**, *44*, 4269.

[265] H. Zhu, F. Yi, E. Cubukcu, *Nat. Photonics* **2016**, *10*, 709.

[266] M. Barbuto, A. Monti, F. Bilotti, A. Toscano, *IEEE Trans. Antennas Propag.* **2013**, *61*, 1219.

[267] L. Luo, I. Chatzakis, J. Wang, F. B. P. Niesler, M. Wegener, T. Koschny, C. M. Soukoulis, *Nat. Commun.* **2014**, *5*, 3055.

**ADVANCED
SCIENCE NEWS**

www.advancedsciencenews.com

**ADVANCED
MATERIALS**

www.advmat.de

[268] M. Fang, K. Niu, Z. Huang, W. E. I. Sha, X. Wu, T. Koschny, C. M. Soukoulis, *Opt. Express* **2018**, *26*, 14241.

[269] A. Singh, A. Pashkin, S. Winnerl, M. Helm, H. Schneider, *ACS Photonics* **2018**, *5*, 2718.

[270] B. Xiong, L. Deng, R. W. Peng, Y. Liu, *Nanoscale Adv.* **2019**, *1*, 3786.

[271] R. Won, *Nat. Photonics* **2018**, *12*, 130.

[272] T. Zentgraf, *Nat. Nanotechnol.* **2018**, *13*, 179.

[273] S. Shrestha, A. C. Overvig, M. Lu, A. Stein, N. Yu, *Light: Sci. Appl.* **2018**, *7*, 85.

[274] W. T. Chen, A. Y. Zhu, J. Sisler, Z. Bharwani, F. Capasso, *Nat. Commun.* **2019**, *10*, 355.

[275] X. Y. Hu, P. Jiang, C. Y. Ding, H. Yang, Q. H. Gong, *Nat. Photonics* **2008**, *2*, 185.

[276] N. I. Zheludev, Y. S. Kivshar, *Nat. Mater.* **2012**, *11*, 917.

[277] F.-Z. Shu, F.-F. Yu, R.-W. Peng, Y.-Y. Zhu, B. Xiong, R.-H. Fan, Z.-H. Wang, Y. Liu, M. Wang, *Adv. Opt. Mater.* **2018**, *6*, 1700939.

[278] M. Liu, H. Y. Hwang, H. Tao, A. C. Strikwerda, K. Fan, G. R. Keiser, A. J. Sternbach, K. G. West, S. Kittiwatanakul, J. Lu, S. A. Wolf, F. G. Omenetto, X. Zhang, K. A. Nelson, R. D. Averitt, *Nature* **2012**, *487*, 345.

[279] H. Abbaszadeh, A. Souslov, J. Paulose, H. Schomerus, V. Vitelli, *Phys. Rev. Lett.* **2017**, *119*, 195502.

[280] S. A. Cummer, J. Christensen, A. Alù, *Nat. Rev. Mater.* **2016**, *1*, 16001.

[281] G. Ma, P. Sheng, *Sci. Adv.* **2016**, *2*, e1501595.

[282] J. H. Lee, J. P. Singer, E. L. Thomas, *Adv. Mater.* **2012**, *24*, 4782.

[283] C. Z. Fan, Y. Gao, J. P. Huang, *Appl. Phys. Lett.* **2008**, *92*, 251907.

[284] M. Kadic, T. Bückmann, R. Schittny, M. Wegener, *Rep. Prog. Phys.* **2013**, *76*, 126501.

1904646 (22 of 22)